JOURNAL OF MATERIALS SCIENCE **41** (2006) 229–249

Effect of electrical conductivity on poling and the dielectric, pyroelectric and piezoelectric properties of ferroelectric 0-3 composites

C. K. WONG
Department of Applied Physics, The Hong Kong Polytechnic University, Hong Kong, China

F. G. SHIN
Department of Applied Physics, Materials Research Center and Center for Smart Materials, The Hong Kong Polytechnic University, Hong Kong, China

We have investigated the effects of electrical conductivity of the constituents on the poling behavior, dielectric, pyroelectric and piezoelectric properties of ferroelectric 0-3 composites. Modeling of polarization behavior is explored for both dc and ac poling procedures. Simulated results show that, in addition to the poling schedule, conductivity plays an important role in the poling process. Calculations are carried out for the time dependent internal electric fields induced by an ac field in dielectric measurements, by modulated temperature in pyroelectric measurement or by stress in piezoelectric measurement. Our previously developed models for dielectricity, pyroelectricity and piezoelectricity have been extended to include the additional contribution from the electrical conductivities. These can be significant for ceramic/polymer composites possessing high conductivity in the matrix phase. Calculated values based on the new model are discussed and compared with the previous models, and in particular the pyroelectric activities reported in the literature for a graphite doped lead zirconate titanate / polyurethane composite. Explicit expressions for the transient and steady state responses are given and the effective permittivity, pyroelectric and piezoelectric coefficients are derived in this paper. Remarkable enhancement in these coefficients is obtained when higher conductivity is introduced in the matrix phase.

1. Introduction

One of the primary goals of embedding ferroelectric ceramic particles within a polymer matrix (i.e. to form a 0-3 composite) is to combine the better properties of ceramic and polymer. Ferroelectric ceramics have high piezoelectric and pyroelectric properties, but their poor mechanical properties and the large difference in acoustic impedance with water and human tissues tend to restrict their usefulness in many applications. Ferroelectric polymers, on the other hand, have good mechanical flexibility, but their piezoelectric and pyroelectric coefficients are low. The use of ferroelectric composites seems capable of overcoming these deficiencies and their properties can be tailored for specific situations. One may in principle design a 0-3 composite with high ceramic volume fraction for applications necessitating high piezoelectric and pyroelectric values. However, it is difficult to fabricate a 0-3 composite sample of high ceramic concentration and the high ceramic content will also lower the flexibility of the composite.

In an interesting paper [1], Chen *et al.* reported very high piezoelectric coefficients of a solvent treated ferroelectric 0-3 composite. They immersed the composite sample of lead zirconate titanate/polyvinylidene fluoride (PZT/PVDF) in a solvent [e.g., *N*-dimethylacetamide] for a period of time. The piezoelectric and dielectric properties were measured after the sample was removed from the solvent environment. They observed that both the permittivity and d_{33} coefficient were significantly larger than those of the virgin specimen. Such high values are quite likely to be out of reach of existing model predictions for "normal" dielectric and piezoelectric 0-3 composites. We have suggested

0022-2461
DOI: 10.1007/s10853-005-7243-3

in a previous paper [2] that these enhancements could very well be related to an increased of electrical conductivity in the matrix material brought about by the solvent.

Indeed, the effect of higher conductivity in the polymer matrix is not limited only to enhancing the pyroelectric and piezoelectric properties. Recently we find that, in the poling process of ferroelectric composites, it shortens the time development of the electric field acting on the ceramic to reach saturation, therefore poling of the ceramic phase in such composite systems can be more efficient [3, 4], which is of practical significance since the pyroelectric and piezoelectric activities of the constituents are generally proportional to their degree of poling [4, 5]. Sakamoto *et al.* [6] also attempted to improve the poling efficiency of lead zirconate titanate/polyurethane (PZT/PU) 0-3 composites by doping with graphite filler. By adding about 1% by volume of graphite to increase the electrical conductivity of PU, the poling of the PZT phase becomes easier. In addition, they also observed that the pyroelectric and piezoelectric d_{33} coefficients of the graphite doped composite show superior properties over their undoped samples.

The study of the poling process is highly important since an understanding of the physical processes behind poling will be useful for the selection of materials and the poling method of composite systems for particular applications. In one poling format of a ferroelectric ceramic/polymer composite, the ceramic phase is first polarized under a dc field for a certain duration at temperatures higher than the Curie transition temperature of the polymer phase, then the polymer phase is polarized under a constant field at decreasing temperature. The large deviation between the permittivities of the ferroelectric ceramic and the polymer will lead to a large difference in the electric field acting on the two phases. In this context, it is difficult to simultaneously obtain a high poling degree for both phases. Recently, it was suggested that the polymer phase could be polarized under an ac field; the ac field does not polarize the ceramic phase if the poling duration is substantially shorter than the dielectric relaxation time of charge in the composite [7, 8]. In other words, a two stage poling process can be employed, i.e., a dc poling at elevated temperature followed by an ac poling at a lower temperature. In this article, theoretical simulations of dc poling, ac poling and their combinations are performed for different poling formats/schedules. The effect of electrical conductivity on the poling results of composites with low and medium high ceramic volume fractions will be discussed.

This paper also attempts to investigate the effect of electrical conductivity on the dielectric, pyroelectric and piezoelectric properties of a ferroelectric composite of a dispersion of spherical inclusions in a continuous matrix, assuming the constituents possess finite conductivity. The sample is excited by an ac electric field of small amplitude or stress for dielectric and piezoelectric measurement, whilst for pyroelectric measurement the sample is excited by an ac modulated or linearly ramped temperature. An analytical model is given and explicit expressions are derived for the dynamic behavior of the electric fields in the constituents. The steady state solutions are then used to obtain explicit expressions for the effective permittivity, pyroelectric and piezoelectric coefficients. Compared to our previously derived analytical expressions for permittivity [9], pyroelectricity [10], and piezoelectricity [11] which assume perfectly insulating constituents, the new set of expressions contains a new factor describing the coupled effects of permittivity, conductivity and the measuring frequency. A generalization of the effective permittivity expression for the concentrated suspension regime is also given by the present model. To illustrate the various new results, theoretical evaluations based on typical ferroelectric composites (e.g. PZT/PVDF) are discussed. Sakamoto *et al.* reported a monotonic increasing profile of pyroelectric coefficients when their PZT/PU sample was heated at a constant rate [6]. This can also be qualitatively simulated by assuming an increase in the conductivity of PU. We will demonstrate that this enhancement is significant for samples with a moderately conductive matrix phase.

2. Theory

To model the polarization behavior and to find the effective permittivity, pyroelectric and piezoelectric coefficients of a 0-3 composite of two ferroelectric phases, we first obtain the time development of the internal electric fields within the individual phases, given the external sinusoidal electric field, modulating temperature or stress. Then the poling process can be modeled and the steady state solution of the in-phase component of internal fields will be used to obtain expressions for the permittivity, pyroelectric and piezoelectric coefficients.

2.1. A formulation for calculating the dynamic behavior of internal electric fields

Suppose the composite is initially polarized in the z direction, in which case we only need to be concerned with the electric field and polarization in the "3" direction. We first write the volumetric average electric displacement D and conduction current density j for the ferroelectric constituent materials in the composite as [12]

$$\begin{cases} \langle D_{3i} \rangle = \varepsilon_i \langle E_{3i} \rangle + \langle P_{3i} \rangle \\ \langle D_{3m} \rangle = \varepsilon_m \langle E_{3m} \rangle + \langle P_{3m} \rangle \end{cases}, \tag{1}$$

$$\begin{cases} \langle j_{3i} \rangle = \sigma_i \langle E_{3i} \rangle \\ \langle j_{3m} \rangle = \sigma_m \langle E_{3m} \rangle \end{cases}, \tag{2}$$

where the angular brackets denote volume-averaged fields enclosed. P is polarization, ε and σ denote permittivity and electrical conductivity respectively, and E is electric field. Subscripts i and m denote "inclusion" and "matrix" respectively.

Consider the single inclusion problem of a ferroelectric sphere surrounded by a ferroelectric matrix medium with a uniform electric field applied along the 3-direction far away from the inclusion. The boundary value problem gives the following equations (see ref. [12]):

$$\langle D_{3i}\rangle + 2\varepsilon_m\left(\langle E_{3i}\rangle - \langle E_{3m}\rangle\right) = \langle D_{3m}\rangle - q_0, \quad (3)$$

$$\langle j_{3i}\rangle + 2\sigma_m\left(\langle E_{3i}\rangle - \langle E_{3m}\rangle\right) = \langle j_{3m}\rangle + \partial q_0/\partial t. \quad (4)$$

In Equations 3 and 4, we have assumed both constituent materials are uniformly polarized and the homogeneously polarized sphere is covered with surface charge of density q_0 at the pole along the polarizing direction ($\theta = 0$) with a distribution given by $q_0 \cos\theta$.

In a previous paper [9], Poon and Shin considered nonferroelectric composites of zero conductivities (where $\langle P_{3i}\rangle = \langle P_{3m}\rangle = 0$ and $q_0 = 0$). They suggested Equation 3 can be written more accurately as

$$\langle D_{3i}\rangle + 2\varepsilon_m\left(\langle E_{3i}\rangle - \langle E_{3m}\rangle\right) = \langle \tilde{D}_{3m}\rangle \quad (5)$$

at higher volume fraction ϕ of inclusions, where $\langle \tilde{D}_3 m\rangle$ is the electric displacement of the surrounding matrix material as seen by a particular single inclusion in the composite. It has two contributions (the pure medium and the polarization from other inclusions):

$$\langle D_{3m}\rangle = \langle D_{3m}\rangle + \phi\,\langle P_{3i}\rangle\,, \quad (6)$$

where $\langle \tilde{P}_{3i}\rangle = (\varepsilon_i - \varepsilon_m)\langle E_{3i}\rangle$. For a ferroelectric composite with interfacial charge accumulation, Equation 5 may be rewritten, following the same rationale, as

$$\langle D_{3i}\rangle + 2\varepsilon_m\left(\langle E_{3i}\rangle - \langle E_{3m}\rangle\right) = \langle D_{3m}\rangle - q_0, \quad (7)$$

where $\langle \tilde{D}_{3m}\rangle = \langle D_{3m}\rangle + \phi\langle \tilde{P}^f_{3i}\rangle$ and $\langle \tilde{P}^f_{3i}\rangle = \langle P_{3i}\rangle - \langle P_{3m}\rangle + q_0 + (\varepsilon_i - \varepsilon_m)\langle E_{3i}\rangle$. Hence, Equation 4 may also be rewritten for higher volume fraction as

$$\langle j_{3i}\rangle + 2\sigma_m\left(\langle E_{3i}\rangle - \langle E_{3m}\rangle\right) = \langle j_{3m}\rangle + \phi\left(\sigma_i - \sigma_m\right)\langle E_{3i}\rangle + (1-\phi)\,\partial q_0/\partial t. \quad (8)$$

For a composite comprising spherical particles uniformly distributed in the matrix material, the volumetric averages of the electric fields satisfy [9, 11]

$$\langle E_3\rangle = \phi\langle E_{3i}\rangle + (1-\phi)\langle E_{3m}\rangle. \quad (9)$$

We can then obtain from Equations 1, 2, 7–9

$$\frac{\partial\langle E_{3i}\rangle}{\partial t} + \frac{\langle E_{3i}\rangle}{\tau} = \frac{3[\sigma_m\langle E_3\rangle + \varepsilon_m\partial\langle E_3\rangle/\partial t] + (1-\phi)^2\,\partial[\langle P_{3m}\rangle - \langle P_{3i}\rangle]/\partial t}{\phi 3\varepsilon_m + (1-\phi)\{\varepsilon_i + 2\varepsilon_m - \phi(\varepsilon_i - \varepsilon_m)\}}, \quad (10)$$

where

$$\tau = \frac{\phi 3\varepsilon_m + (1-\phi)\{\varepsilon_i + 2\varepsilon_m - \phi(\varepsilon_i - \varepsilon_m)\}}{\phi 3\sigma_m + (1-\phi)\{\sigma_i + 2\sigma_m - \phi(\sigma_i - \sigma_m)\}}. \quad (11)$$

2.2. Modeling the hysteresis behavior of a ferroelectric composite

Equation 10 is a first order differential equation. For a given external field, which may be equated to $\langle E_3\rangle$, we may obtain $\langle E_{3i}\rangle$ as a function of time t when the P-E relations for the individual constituents ($\langle P_{3i}\rangle$ versus $\langle E_{3i}\rangle$ and $\langle P_{3m}\rangle$ versus $\langle E_{3m}\rangle$) are known. The P-E relationship of a ferroelectric material is very complex and it has been the subject of many investigations. The ferroelectric polarization is generally not a simple function of the electric field. The change of polarization depends on a change of electric field as well as on the polarization already present. Here we use the model of Miller *et al.* to describe P-E relations of the constituent materials [13, 14]:

$$\frac{\partial P}{\partial E} = \left(1 - \tanh\sqrt{\frac{P - P_{sat}}{\xi P_s - P}}\right)\left(\frac{\partial P_{sat}}{\partial E}\right), \quad (12)$$

where P_{sat} is the polarization of the saturated hysteresis loop at the field of interest, and P and P_s are the magnitudes of the ferroelectric polarization and saturation polarization, respectively. In this model, ξ takes $+1$ and -1 for increasing E and decreasing E respectively. The polarization of the saturated hysteresis loop is written as a function of the electric field as

$$P_{sat} = \xi P_s \tanh\left\{\frac{\xi E - E_c}{2E_c}\ln\left(\frac{1 + P_r/P_s}{1 - P_r/P_s}\right)\right\}, \quad (13)$$

where P_r and E_c are taken as positive quantities representing the magnitude of remanent polarization and coercive field, respectively. Since different kinds of ferroelectric materials may have different hysteresis loop shapes (corresponding to different $\partial P/\partial E$ for a given field), even though they may have the same values of P_r, P_s and E_c, we have therefore slightly modified Equation 13 to include a factor $n \equiv n_1/n_2$ to extend the usage of Miller

et al.'s model for a broader range of ferroelectrics, and as a result the saturated hysteresis loop may be written as

$$P_{sat} = \xi P_s \tanh\left\{\frac{\xi E - E_c}{2E_c} \ln\left[\frac{1-(-P_r/P_s)^{1/n}}{1+(-P_r/P_s)^{1/n}}\right]\right\}^n. \quad (14)$$

In general, it is found that odd-numbered n_1 and n_2 with n_1/n_2 ranging from 1/3 to 1 will give results close to hysteresis loops of realistic materials. When Equation 12 is solved with Equation 10, the relations $\partial\langle P_{3i}\rangle/\partial t = [\partial\langle P_{3i}\rangle/\partial\langle E_{3i}\rangle][\partial\langle E_{3i}\rangle/\partial t]$ and $\partial\langle P_{3m}\rangle/\partial t = [\partial\langle P_{3m}\rangle/\partial\langle E_{3m}\rangle][\partial\langle E_{3m}\rangle/\partial t]$ should be employed. Concerning the initial condition of internal fields, our theoretical calculations assume electric fields in the constituents are both initially zero.

2.3. Effective permittivity of a ferroelectric 0-3 composite

For dielectric measurement, assume $\langle E_3\rangle = E_0 \sin \omega t$ where $\omega = 2\pi f$ and f is the frequency of the applied field. We further assume the amplitude E_0 is small such that the contribution from the hysteresis behavior may be neglected. Thus, $\partial\langle P_{3m}\rangle/\partial t = \partial\langle P_{3i}\rangle/\partial t = 0$ in Equation 10 which becomes

$$\frac{\partial\langle E_{3i}\rangle}{\partial t} + \frac{\langle E_{3i}\rangle}{\tau} = L_E\left\{\frac{\partial\langle E_3\rangle}{\partial t} + \frac{\langle E_3\rangle}{\tau_m}\right\}, \quad (15)$$

where $\tau_m = \varepsilon_m/\sigma_m$ and

$$L_E = \frac{3\varepsilon_m}{\phi 3\varepsilon_m + (1-\phi)\{\varepsilon_i + 2\varepsilon_m - \phi(\varepsilon_i - \varepsilon_m)\}}. \quad (16)$$

Assuming $\langle E_{3i}\rangle$ is initially zero, the solution from solving Equation 15 is:

$$\langle E_{3i}\rangle = \left(\frac{E_0\tau/\tau_m}{1+\omega^2\tau^2}\right) L_E\{\omega(\tau-\tau_m)e^{-t/\tau} + (1+\omega^2\tau\tau_m)\sin\omega t - \omega(\tau-\tau_m)\cos\omega t\}. \quad (17)$$

In a dielectric measurement, the electric current flowing in the composite is used to determine the permittivity value. The volumetric average of the total current density is

$$\langle J_3\rangle = \langle j_3\rangle + \partial\langle D_3\rangle/\partial t, \quad (18)$$

where

$$\begin{cases}\langle j_3\rangle = \phi\langle j_{3i}\rangle + (1-\phi)\langle j_{3m}\rangle \\ \langle D_3\rangle = \phi\langle D_{3i}\rangle + (1-\phi)\langle D_{3m}\rangle\end{cases}. \quad (19)$$

At sufficiently long time from the start of the dielectric measurement (i.e. at steady state), the term $\exp(-t/\tau)$ in Equation 17 may be omitted. The components of $\langle E_{3i}\rangle$ in phase and 90° out of phase with the applied field are

$$\langle E_{3i}\rangle|_{\text{in phase}} = \left(\frac{E_0\tau/\tau_m}{1+\omega^2\tau^2}\right) \times L_E\{(1+\omega^2\tau\tau_m)\sin\omega t\}, \quad (20)$$

$$\langle E_{3i}\rangle|_{\text{out of phase}} = \left(\frac{E_0\tau/\tau_m}{1+\omega^2\tau^2}\right) \times L_E\{\omega(\tau_m-\tau)\cos\omega t\}. \quad (21)$$

In this paper, we only focus on the in-phase component of the dielectric property. The permittivity is thus:

$$\varepsilon = \frac{\partial\left\{\int\langle J_3\rangle dt\right\}_{\text{in phase}}}{\partial\langle E_3\rangle}. \quad (22)$$

Substituting Equations 18–20 into Equation 22 and making use of Equations 1, 2, 9, the effective permittivity is obtained as:

$$\varepsilon = \varepsilon_m + \phi\Gamma_\varepsilon L_E(\varepsilon_i - \varepsilon_m), \quad (23)$$

where

$$\Gamma_\varepsilon = \frac{\tau\{\tau_m^{-1} + \tau_{neg}^{-1}(1-\tau/\tau_m)\} + \omega^2\tau^2}{1+\omega^2\tau^2}, \quad (24)$$

$$\tau_{neg} = \frac{\varepsilon_i - \varepsilon_m}{\sigma_i - \sigma_m}, \quad (25)$$

or in a more compact form:

$$\varepsilon = \varepsilon_m \frac{(\varepsilon_i + 2\varepsilon_m) + \{3\Gamma_\varepsilon - (2-\phi)\}\phi(\varepsilon_i - \varepsilon_m)}{(\varepsilon_i + 2\varepsilon_m) - \phi(2-\phi)(\varepsilon_i - \varepsilon_m)}. \quad (26)$$

Note that when $\sigma_i = \sigma_m = 0$, then $\Gamma = 1$ and Equation 26 reduces to

$$\varepsilon = \varepsilon_m \frac{(\varepsilon_i + 2\varepsilon_m) + \phi(1+\phi)(\varepsilon_i - \varepsilon_m)}{(\varepsilon_i + 2\varepsilon_m) - \phi(2-\phi)(\varepsilon_i - \varepsilon_m)}. \quad (27)$$

This equation is identical to the permittivity formula suggested by Poon and Shin [9].

2.4. Effective pyroelectric coefficient of a ferroelectric 0-3 composite

The polarization of a ferroelectric material will be influenced by temperature (pyroelectricity) and stress (piezoelectricity). We will first derive the pyroelectric coefficient

which is measured by using an ac temperature modulation, then by a direct method using constant heating rate. In each case the pyroelectric current is determined.

2.4.1. Sinusoidally modulated temperature method

In the pyroelectric measurement, the polarizations $\langle P_{3i}\rangle$ and $\langle P_{3m}\rangle$ vary with the temperature modulation. Suppose the composite is subjected to a sinusoidal temperature Θ. The rates of change of polarizations in Equation 10 are related to the temperature due to pyroelectric effect:

$$\left\{ \frac{\partial \langle P_{3i}\rangle}{\partial t} = p_i \frac{\partial \Theta}{\partial t},\ \frac{\partial \langle P_{3m}\rangle}{\partial t} = p_m \frac{\partial \Theta}{\partial t} \right. , \tag{28}$$

where p denotes pyroelectric coefficient.

In short-circuit condition (i.e., $\langle E_3\rangle = 0$), Equation 10 becomes

$$\frac{\partial \langle E_{3i}\rangle}{\partial t} + \frac{\langle E_{3i}\rangle}{\tau} = \frac{(1-\phi)^2 (p_m - p_i)}{\phi 3\varepsilon_m + (1-\phi)\{\varepsilon_i + 2\varepsilon_m - \phi(\varepsilon_i - \varepsilon_m)\}} \frac{\partial \Theta}{\partial t}. \tag{29}$$

Assuming $\Theta = \Theta_0 \sin \omega t$ with Θ_0 being the amplitude of modulation temperature and $\langle E_{3i}\rangle$ initially zero, the solution from solving Equation 29 is:

$$\langle E_{3i}\rangle = \left(\frac{\Theta_0 \omega\tau}{1+\omega^2\tau^2}\right) \times \frac{(1-\phi)^2 (p_m - p_i)}{\phi 3\varepsilon_m + (1-\phi)\{\varepsilon_i + 2\varepsilon_m - \phi(\varepsilon_i - \varepsilon_m)\}} \times (\omega\tau \sin \omega t + \cos \omega t - e^{-t/\tau}), \tag{30}$$

where $\omega = 2\pi f$ and f is the frequency of modulated temperature. From Equation 9, $\langle E_{3m}\rangle = -\phi\langle E_{3i}\rangle/(1-\phi)$, since $\langle E_3\rangle = 0$ in pyroelectric measurement.

For a sufficiently long time in the pyroelectric measurement (i.e. at steady state), the term $\exp(-t/\tau)$ in Equation 30 may be neglected. The components of $\langle E_{3i}\rangle$ in phase and 90° out of phase with the modulated temperature are

$$\langle E_{3i}\rangle|_{\text{in phase}} = \left(\frac{\Theta_0 \omega^2\tau^2}{1+\omega^2\tau^2}\right) \times \frac{(1-\phi)^2 (p_m - p_i) \sin \omega t}{\phi 3\varepsilon_m + (1-\phi)\{\varepsilon_i + 2\varepsilon_m - \phi(\varepsilon_i - \varepsilon_m)\}}, \tag{31}$$

$$\langle E_{3i}\rangle|_{\text{out of phase}} = \left(\frac{\Theta_0 \omega\tau}{1+\omega^2\tau^2}\right) \times \frac{(1-\phi)^2 (p_m - p_i) \cos \omega t}{\phi 3\varepsilon_m + (1-\phi)\{\varepsilon_i + 2\varepsilon_m - \phi(\varepsilon_i - \varepsilon_m)\}}. \tag{32}$$

Again, we only focus on the in-phase component. The pyroelectric coefficient of the composite is calculated from:

$$p = \frac{\partial\{\int \langle J_3\rangle dt\}_{\text{in phase}}}{\partial \Theta}. \tag{33}$$

Note that this corresponds to the pyroelectric current which is out-of-phase with the temperature modulation, as measured in practice. Substituting Equation 31 into Equations 1, 2 and 18, we obtain from Equation 33

$$p = \phi p_i + (1-\phi) p_m + \phi(1-\phi)\Gamma_p^{\text{ac}} \times (L_E - \bar{L}_E)(p_i - p_m), \tag{34}$$

where

$$\Gamma_p^{\text{ac}} = \frac{\tau/\tau_{neg} + \omega^2\tau^2}{1+\omega^2\tau^2}, \tag{35}$$

$$\bar{L}_E = \frac{1-\phi L_E}{1-\phi} = \frac{(1-\phi)\varepsilon_i + (2+\phi)\varepsilon_m}{\phi 3\varepsilon_m + (1-\phi)\{\varepsilon_i + 2\varepsilon_m - \phi(\varepsilon_i - \varepsilon_m)\}}. \tag{36}$$

Alternatively, the effective pyroelectric coefficient can be re-expressed as

$$p = \phi[1 - \Gamma_p^{\text{ac}}(1 - L_E)]p_i + (1-\phi)[1 - \Gamma_p^{\text{ac}}(1 - \bar{L}_E)]p_m. \tag{37}$$

Note that when $\sigma_i = \sigma_m = 0$, we have $\Gamma_p^{\text{ac}} = 1$ and Equation 37 reduces to:

$$p = \phi L_E p_i + (1-\phi)\bar{L}_E p_m, \tag{38}$$

which is the familiar form for pyroelectric coefficient suggested in the literature [15–17]. If one follows the same footsteps to solve the pyroelectric coefficient but using Equations 3 and 4 rather than Equations 7 and 8 (i.e. for low ϕ), expressions for L_E and $\bar{L}_E$ become the pair derived

previously [11, 12, 18, 19] and Equation 38 will be identical to the formula for primary pyroelectric coefficient suggested by Chew *et al.* [10].

Equation 37 is also a generalization of the expression suggested by Lam *et al.* who investigated the pyroelectric properties of dilute (small ϕ) composites with non-pyroelectric matrix [19].

2.4.2. Linear temperature ramp method

For the pyroelectric measurement with the sample being heated at a constant rate, Θ can be written as $\Theta = \Theta_{rm} + \Re_\Theta t$ with Θ_{rm} and $\Re_\Theta$ being the initial temperature and heating rate respectively.

Assuming $\langle E_{3i}\rangle$ is initially zero, the solution from solving Equation 29 now becomes:

$$\langle E_{3i}\rangle = \frac{(1-\phi)^2(p_m - p_i)\Re_\Theta \tau}{\phi 3\varepsilon_m + (1-\phi)\{\varepsilon_i + 2\varepsilon_m - \phi(\varepsilon_i - \varepsilon_m)\}} \times (1 - e^{-t/\tau}), \tag{39}$$

and $\langle E_{3m}\rangle = -\phi\langle E_{3i}\rangle/(1-\phi)$, since $\langle E_3\rangle = 0$ in pyroelectric measurement.

From Equations 1, 2, 18 and 39, the pyroelectric current of the composite obtained from measurement is derived as:

$$I_p = \Re_\Theta A\{\phi p_i + (1-\phi)\, p_m + \phi(1-\phi)\,\Gamma_p^{\text{ramp}} \times (L_E - \bar{L}_E)(p_i - p_m)\}, \tag{40}$$

where A is the electrode area and

$$\Gamma_p^{\text{ramp}} = e^{-t/\tau} + (1 - e^{-t/\tau})\tau/\tau_{neg}. \tag{41}$$

The pyroelectric coefficient is then directly obtained from Equation 40

$$p = \phi p_i + (1-\phi)p_m + \phi(1-\phi) \times \Gamma_p^{\text{ramp}}(L_E - \bar{L}_E)(p_i - p_m). \tag{42}$$

Alternatively, the effective pyroelectric coefficient can be re-expressed as

$$p = \phi[1 - \Gamma_p^{\text{ramp}}(1 - L_E)]p_i + (1-\phi)[1 - \Gamma_p^{\text{ramp}}(1 - \bar{L}_E)]p_m. \tag{43}$$

2.5. Effective piezoelectric coefficients of a ferroelectric 0-3 composite

In the piezoelectric measurement, the polarizations $\langle P_{3i}\rangle$ and $\langle P_{3m}\rangle$ vary with the applied stress. Suppose the composite is subjected to an external tensile stress T. The rates of change of polarizations in Equation 10 can be related to the external stress due to the piezoelectric effect. Thus see ref. 2,

$$\begin{cases} \dfrac{\partial\langle P_{3i}\rangle}{\partial t} = d_i \dfrac{\partial T}{\partial t} \\ \dfrac{\partial\langle P_{3m}\rangle}{\partial t} = d_m \dfrac{\partial T}{\partial t} \end{cases}, \tag{44}$$

where $d_i = \partial\langle P_{3i}\rangle/\partial T$, $d_m = \partial\langle P_{3m}\rangle/\partial T$. When the stress is applied along the x direction, i.e. $T = T_{xx}$, then $d_i = d_i^\perp$ and $d_m = d_m^\perp$, where

$$d_i^\perp = \left(L_T^{/\!/} + L_T^\perp\right) d_{31i} + L_T^\perp d_{33i}, \tag{45}$$

$$d_m^\perp = \left(\bar{L}_T^{/\!/} + \bar{L}_T^\perp\right) d_{31m} + \bar{L}_T^\perp d_{33m}, \tag{46}$$

and

$$L_T^\perp = \frac{I_T}{1-\phi(1-3I_T)} - \frac{J_T}{1-\phi(1-3J_T)}, \tag{47}$$

$$L''_T = \frac{I_T}{1-\phi(1-3I_T)} + \frac{2J_T}{1-\phi(1-3J_T)}, \tag{48}$$

$$\bar{L}_T^\perp = \frac{-\phi L_T^\perp}{1-\phi} = \frac{1}{3}\left[\frac{1}{1-\phi(1-3I_T)} - \frac{1}{1-\phi(1-3J_T)}\right], \tag{49}$$

$$\bar{L}''_T = \frac{1-\phi L''_T}{1-\phi} = \frac{1}{3}\left[\frac{1}{1-\phi(1-3I_T)} + \frac{2}{1-\phi(1-3J_T)}\right], \tag{50}$$

$$I_T = \frac{1}{3}\frac{k_i}{k_m}\frac{3k_m + 4\mu_m}{3k_i + 4\mu_m}, \tag{51}$$

$$J_T = \frac{5}{3}\frac{(3k_m + 4\mu_m)\,\mu_i}{6(k_m + 2\mu_m)\,\mu_i + (9k_m + 8\mu_m)\,\mu_m}. \tag{52}$$

Here d_{31} and d_{33} are the piezoelectric coefficients. k and μ denote bulk modulus and shear modulus respectively.

When the stress acts along the z direction, i.e. $T = T_{zz}$, then $d_i = d_i^{//}$ and $d_m = d_m^{//}$, where

$$d_i^{//} = L_T^{//} d_{33i} + 2L_T^{\perp} d_{31i}, \tag{53}$$

$$d_m^{//} = \bar{L}_T^{//} d_{33m} + 2\bar{L}_T^{\perp} d_{31m}. \tag{54}$$

In short-circuit condition (i.e., $\langle E_3 \rangle = 0$), Equation 10 becomes

$$\frac{\partial \langle E_{3i} \rangle}{\partial t} + \frac{\langle E_{3i} \rangle}{\tau} = \frac{(1-\phi)^2 (d_m - d_i)}{\phi 3\varepsilon_m + (1-\phi)\{\varepsilon_i + 2\varepsilon_m - \phi(\varepsilon_i - \varepsilon_m)\}} \frac{\partial T}{\partial t}. \tag{55}$$

Assuming $T = T_0 \sin \omega t$ with T_0 being the amplitude of applied stress and $\langle E_{3i} \rangle$ initially zero, the solution from solving Equation 55 is:

$$\langle E_{3i} \rangle = \left(\frac{T_0 \omega \tau}{1 + \omega^2 \tau^2} \right) \times \frac{(1-\phi)^2 (d_m - d_i)}{\phi 3\varepsilon_m + (1-\phi)\{\varepsilon_i + 2\varepsilon_m - \phi(\varepsilon_i - \varepsilon_m)\}} \times (\omega\tau \sin \omega t + \cos \omega t - e^{-t/\tau}), \tag{56}$$

where $\omega = 2\pi f$ and f is the frequency of applied stress. From Equation 9, $\langle E_{3m} \rangle = -\phi \langle E_{3i} \rangle / (1-\phi)$, since $\langle E_3 \rangle = 0$ in piezoelectric measurement.

For a sufficiently long time in the piezoelectric measurement, the term $\exp(-t/\tau)$ in Equation 56 drops out. The components of $\langle E_{3i} \rangle$ in phase and 90° out of phase with the applied stress are

$$\langle E_{3i} \rangle|_{\text{in phase}} = \left(\frac{T_0 \omega^2 \tau^2}{1 + \omega^2 \tau^2} \right) \times \frac{(1-\phi)^2 (d_m - d_i) \sin \omega t}{\phi 3\varepsilon_m + (1-\phi)\{\varepsilon_i + 2\varepsilon_m - \phi(\varepsilon_i - \varepsilon_m)\}}, \tag{57}$$

$$\langle E_{3i} \rangle|_{\text{out of phase}} = \left(\frac{T_0 \omega \tau}{1 + \omega^2 \tau^2} \right) \times \frac{(1-\phi)^2 (d_m - d_i) \cos \omega t}{\phi 3\varepsilon_m + (1-\phi)\{\varepsilon_i + 2\varepsilon_m - \phi(\varepsilon_i - \varepsilon_m)\}}. \tag{58}$$

Again, we only focus on the in-phase component of the piezoelectric responses. The piezoelectric d coefficient of the composite obtained from measurement is:

$$d = \frac{\partial \left\{ \int \langle J_3 \rangle \, dt \right\}_{\text{in phase}}}{\partial T}. \tag{59}$$

Substituting Equation 57 into Equations 1, 2 and 18, we obtain from Equation 59

$$d = \phi d_i + (1-\phi) d_m + \phi(1-\phi) \Gamma_d \left(L_E - \bar{L}_E \right) \times (d_i - d_m), \tag{60}$$

where

$$\Gamma_d = \frac{\tau / \tau_{neg} + \omega^2 \tau^2}{1 + \omega^2 \tau^2} = \Gamma_p^{\text{ac}}. \tag{61}$$

Further, using Equations 45, 46, 53 and 54, the effective d_{31} and d_{33} coefficients can be re-expressed as

$$\begin{aligned} d_{31} = {} & \phi[1 - \Gamma_d(1 - L_E)] \\ & \times \{(L_T^{//} + L_T^{\perp}) d_{31i} + L_T^{\perp} d_{33i}\} \\ & + (1-\phi)[1 - \Gamma_d(1 - \bar{L}_E)] \\ & \times \{(\bar{L}_T^{//} + \bar{L}_T^{\perp}) d_{31m} + \bar{L}_T^{\perp} d_{33m}\}, \end{aligned} \tag{62}$$

$$\begin{aligned} d_{33} = {} & \phi \left[1 - \Gamma_d (1 - L_E)\right] \left\{ L_T^{//} d_{33i} + 2L_T^{\perp} d_{31i} \right\} \\ & + (1-\phi)[1 - \Gamma_d(1 - \bar{L}_E)] \\ & \times \left\{ \bar{L}_T^{//} d_{33m} + 2\bar{L}_T^{\perp} d_{31m} \right\}. \end{aligned} \tag{63}$$

The effective hydrostatic piezoelectric d_h coefficient is defined by $d_h = d_{33} + 2d_{31}$ (and similarly for inclusion and matrix), thus:

$$\begin{aligned} d_h = {} & \phi[1 - \Gamma_d(1 - L_E)] L_T^h d_{hi} + (1-\phi) \\ & \times [1 - \Gamma_d(1 - \bar{L}_E)] \bar{L}_T^h d_{hm}, \end{aligned} \tag{64}$$

where

$$\begin{aligned} L_T^h &= 2L_T^{\perp} + L_T^{//} \\ &= \frac{\left(1 + \frac{4}{3}\mu_m / k_m\right)}{\phi\left(1 + \frac{4}{3}\mu_m / k_m\right) + \left(1 - \phi\right)\left(1 + \frac{4}{3}\mu_m / k_i\right)}, \end{aligned} \tag{65}$$

$$\bar{L}_T^h = 2\bar{L}_T^{\perp} + \bar{L}_T^{/\!/} = \frac{1-\phi L_T^h}{1-\phi} = \frac{\left(1+\frac{4}{3}\mu_m/k_i\right)}{\phi\left(1+\frac{4}{3}\mu_m/k_m\right)+(1-\phi)\left(1+\frac{4}{3}\mu_m/k_i\right)}. \tag{66}$$

2.6. Effective piezoelectric coefficients of a composite in terms of effective ε, k and μ

The foregoing Equations 62–64 have considered a higher ϕ treatment for the electric problem [Equations 7 and 8], but the elasticity problem [Equations 45, 46, 53 and 54] is only valid for the dilute suspension regime. One can re-express the L_T's [Equations 47–50 and 65–66] in terms of the effective elastic properties of the composite as in refs. 11 and 20. We here adopt the same "transformed" expressions F_T's which have been demonstrated there to give results which are applicable to higher ϕ, provided that better estimates of effective properties are available. This scheme provides simple and tractable explicit expressions for higher ϕ. Thus Equations 62–64 are transformed to:

$$d_{31} = \phi[1-\Gamma_d(1-L_E)]\left\{\left(F_T^{/\!/}+F_T^{\perp}\right)d_{31i} + F_T^{\perp}d_{33i}\right\} + (1-\phi)\left[1-\Gamma_d(1-\bar{L}_E)\right] \times\left\{\left(\bar{F}_T^{/\!/}+\bar{F}_T^{\perp}\right)d_{31m}+\bar{F}_T^{\perp}d_{33m}\right\}' \tag{67}$$

$$d_{33} = \phi\left[1-\Gamma_d\left(1-L_E\right)\right]\left\{F''_T d_{33i}+2F_T^{\perp}d_{31i}\right\} + (1-\phi)\left[1-\Gamma_d(1-\bar{L}_E)\right] \times\left\{\bar{F}''_T d_{33m}+2\bar{F}_T^{\perp}d_{31m}\right\} \tag{68}$$

$$d_h = \phi\left[1-\Gamma_d\left(1-L_E\right)\right]F_T^h d_{hi} + (1-\phi) \times\left[1-\Gamma_d\left(1-\bar{L}_E\right)\right]\bar{F}_T^h d_{hm}, \tag{69}$$

where

$$F_T^{\perp} = \frac{1}{\phi}\left\{\frac{1}{3}\frac{k^{-1}-k_m^{-1}}{k_i^{-1}-k_m^{-1}} - \frac{1}{3}\frac{\mu^{-1}-\mu_m^{-1}}{\mu_i^{-1}-\mu_m^{-1}}\right\}, \tag{70}$$

$$F''_T = \frac{1}{\phi}\left\{\frac{1}{3}\frac{k^{-1}-k_m^{-1}}{k_i^{-1}-k_m^{-1}} + \frac{2}{3}\frac{\mu^{-1}-\mu_m^{-1}}{\mu_i^{-1}-\mu_m^{-1}}\right\}, \tag{71}$$

$$\bar{F}_T^{\perp} = \frac{-\phi F_T^{\perp}}{1-\phi} = \frac{1}{1-\phi} \times\left\{\frac{1}{3}\frac{k_i^{-1}-k^{-1}}{k_i^{-1}-k_m^{-1}} - \frac{1}{3}\frac{\mu_i^{-1}-\mu^{-1}}{\mu_i^{-1}-\mu_m^{-1}}\right\}, \tag{72}$$

$$\bar{F''}_T = \frac{1-\phi F''_T}{1-\phi} = \frac{1}{1-\phi} \times\left\{\frac{1}{3}\frac{k_i^{-1}-k^{-1}}{k_i^{-1}-k_m^{-1}} + \frac{2}{3}\frac{\mu_i^{-1}-\mu^{-1}}{\mu_i^{-1}-\mu_m^{-1}}\right\}, \tag{73}$$

$$F_T^h = \frac{1}{\phi}\frac{k^{-1}-k_m^{-1}}{k_i^{-1}-k_m^{-1}}, \tag{74}$$

$$\bar{F}_T^h = \frac{1-\phi F_T^h}{1-\phi} = \frac{1}{1-\phi}\frac{k_i^{-1}-k^{-1}}{k_i^{-1}-k_m^{-1}}. \tag{75}$$

Concerning the L_E's, they can also be expressed in terms of the effective dielectric property of the composite i.e. transformed to ℓ_E's following the same procedure as in ref. 2. The results are

$$\ell_E = \frac{1}{\phi\Gamma_\varepsilon}\frac{\varepsilon-\varepsilon_m}{\varepsilon_i-\varepsilon_m}, \tag{76}$$

$$\bar{\ell}_E = \frac{1}{(1-\phi)\bar{\Gamma}_\varepsilon}\frac{\varepsilon_i-\varepsilon}{\varepsilon_i-\varepsilon_m}, \tag{77}$$

where Γ_ε is given by Equation 24,

$$\bar{\Gamma}_\varepsilon = \frac{\tau\{\tau_{pos}^{-1}+\tau_{neg}^{-1}(1-\tau/\tau_{pos})\}+\omega^2\tau^2}{1+\omega^2\tau^2}, \tag{78}$$

and $\tau_{pos} = [(1-\phi)\varepsilon_i+(2+\phi)\varepsilon_m]/[(1-\phi)\sigma_i+(2+\phi)\sigma_m]$. Equations 76 and 77 can be used for analyzing the fractions of applied field distributed to the constituents. ℓ_E and $\bar{\ell}_E$ are essentially $\langle E_{3i}\rangle/\langle E_3\rangle$ and $\langle E_{3m}\rangle/\langle E_3\rangle$ respectively [11].

Note that when $\sigma_i = \sigma_m = 0$, $\Gamma_d = 1$ and Equations 67–69 reduce to:

$$d_{31} = \phi F_E\left\{\left(F_T^{/\!/}+F_T^{\perp}\right)d_{31i}+F_T^{\perp}d_{33i}\right\} + (1-\phi)\bar{F}_E\left\{\left(\bar{F}_T^{/\!/}+\bar{F}_T^{\perp}\right)d_{31m} + \bar{F}_T^{\perp}d_{33m}\right\}, \tag{79}$$

$$d_{33} = \phi F_E \left\{ F_T^{//} d_{33i} + 2F_T^{\perp} d_{31i} \right\} + (1-\phi)\bar{F}_E \left\{ \bar{F}_T^{//} d_{33m} + 2\bar{F}_T^{\perp} d_{31m} \right\}, \quad (80)$$

$$d_h = \phi F_E F_T^h d_{hi} + (1-\phi)\bar{F}_E \bar{F}_T^h d_{hm}, \quad (81)$$

where

$$F_E = \frac{1}{\phi} \frac{\varepsilon - \varepsilon_m}{\varepsilon_i - \varepsilon_m}, \quad (82)$$

$$\bar{F}_E = \frac{1-\phi F_E}{1-\phi} = \frac{1}{1-\phi} \frac{\varepsilon_i - \varepsilon}{\varepsilon_i - \varepsilon_m}, \quad (83)$$

which are the ℓ_E's with$\Gamma_\varepsilon = \bar{\Gamma}_\varepsilon = 1$. Equations 79–81 are identical to our previous model [11].

Theoretical predictions given by Equations 67–69 require the values of the bulk modulus and shear modulus of the composite. Sometimes the elastic properties of the composite are not measured together with the piezoelectric properties. In such cases, we can follow the same technique as in our previous articles [11, 20]. For the effective bulk modulus k,

$$k = k_m + \frac{\phi(k_i - k_m)}{1 + (1-\phi)(k_i - k_m)/(k_m + 4\mu_m/3)} \quad (84)$$

gives a good approximation for a composite with spherical inclusions [21]. For the effective shear modulus μ, explicit bounds may be employed. Following Christensen [22], the lower bound μ_l:

$$\mu_l = \mu_m \left\{ 1 + \frac{15(1-\nu_m)(\mu_i/\mu_m - 1)\phi}{7 - 5\nu_m + 2(4-5\nu_m)[\mu_i/\mu_m - (\mu_i/\mu_m - 1)\phi]} \right\} \quad (85)$$

given by Hashin and Shtrikman [23] for arbitrary phase geometry is adopted in our prediction. In Equation 85, ν_m is Poisson's ratio of the matrix phase. The upper bound μ_u given by Hashin for spherical inclusion geometry may also be adopted [21]. If both upper bound μ_u and lower bound μ_l are simultaneously adopted for the effective shear modulus, each prediction of d_{31} and d_{33} coefficients [Equations 67 and 68 respectively] then gives a pair of lines. In the next section, we will only adopt lower bound μ_l to evaluate the effective piezoelectric coefficients, since the resultant pair of lines given by the prediction of piezoelectric coefficients are narrow.

In summary, Equation 26 is used for the prediction of effective permittivity. For pyroelectric measurement using ac modulated temperature, Equation 37 is used. When the linear temperature ramp method is adopted, Equation 43 is to be used accordingly. For piezoelectric coefficients, Equations 67, 68 and 69 are used for the prediction of d_{31}, d_{33} and d_h respectively.

3. Results and discussion

In this section, we will first concentrate on the simulation of poling of ferroelectric 0-3 composites, then the theoretical predictions based on the foregoing formulas for dielectric, pyroelectric and piezoelectric properties are investigated. We will show that electrical conductivity in the matrix phase plays a significant role in influencing those properties.

3.1. Polarization behavior of ferroelectric 0-3 composites

In poling, normally a dc electric field is applied on the ferroelectric sample to force the dipoles to align. It is important to choose an appropriate poling field, temperature and time for a particular ferroelectric sample because the ferroelectric response varies among different materials. To obtain an optimal degree of poling, the poling field should be high (but below the breakdown field of the material) and the poling time should be long enough to get an appreciable stable polarization. For ferroelectric composites of ceramic inclusions dispersed in the polymer matrix, the selection of poling parameters will be more complicated since we cannot directly measure the internal field distribution to properly select the parameters. Theoretical simulation results of poling will be useful as a reference. The discussion of the effects of poling field and poling time have been systemically investigated before [4, 7]. The following discussions will focus on the effects of σ_m and the applied field schedule.

Fig. 1 shows the simulation results of lead zirconate titanate (PZT)/polyvinylidene fluoride-trifluoroethylene [P(VDF-TrFE)] 0-3 composites. The adopted properties for the constituents are shown in Table I. The composites are polarized by a dc electric field of 60 MV/m for an hour with the poled samples then short-circuited for 2 h. This process tends to polarize the two ferroelectric phases in the same direction. Two different conductivity values for the P(VDF-TrFE) copolymer have been adopted to demonstrate the effect of σ_m. σ_i is set to $10^{-12}\ \Omega^{-1}\mathrm{m}^{-1}$, which is small, so that the effect of σ_i is effectively ignored (actually, the poling behavior to be shown below will not be significantly affected by a higher σ_i). In the figures, the solid and dashed lines are used to denote the results for higher and lower σ_m respectively. In Fig. 1a which takes $\phi = 0.1$, the poling in both phases is shown to behave quite differently for lower and higher σ_m. When $\sigma_m = 10^{-14}\ \Omega^{-1}\mathrm{m}^{-1}$ which is smaller than

TABLE I Properties of constituents for PZT/P(VDF-TrFE) 0-3 composites

	$\varepsilon/\varepsilon_0$	σ ($\Omega^{-1}m^{-1}$)	P_r (C/m^2)	P_s (C/m^2)	E_c (MV/m)	n [in Equation 14]
PZT	1600	10^{-12}	0.33	0.35	1	1
P(VDF-TrFE)	20	varied	0.055	0.06	60	1

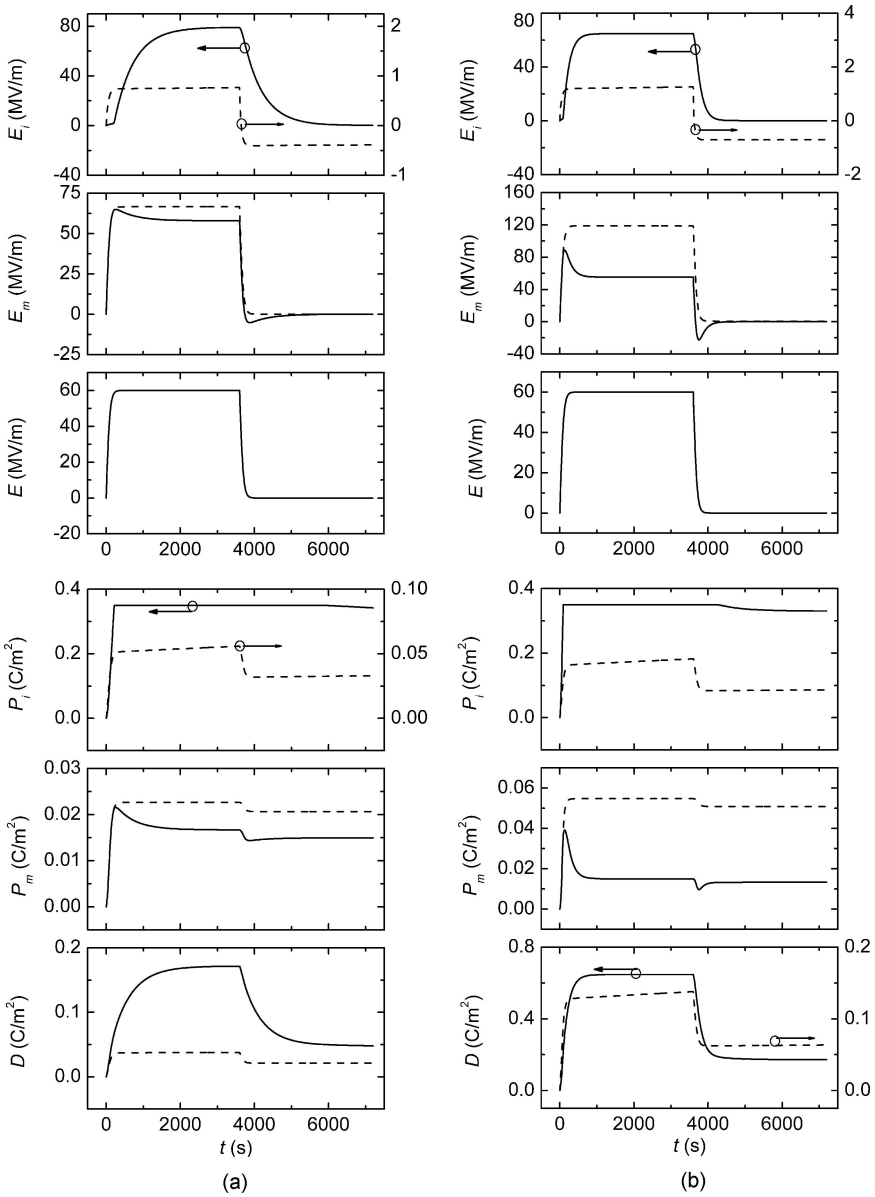

Figure 1 Simulated polarizations and electric fields of PZT/P(VDF-TrFE) composites with (a) ϕ =0.1, (b) $\phi = 0.5$, when the composites are polarized by a dc electric field. The dashed and solid lines denote $\sigma_m = 10^{-14}\Omega^{-1}m^{-1}$ and $\sigma_m = 10^{-11}\Omega^{-1}m^{-1}$ respectively.

σ_i, the degree of poling in PZT is negligibly small, but the copolymer phase is polarized to some extent. When $\sigma_m = 10^{-11}$ $\Omega^{-1}m^{-1}$, the situation is changed: the degree of poling in PZT is satisfactory, although the degree of poling in the copolymer phase is still restricted. For a higher ceramic volume fraction, Fig. 1b shows the simulation results of a composite ($\phi = 0.5$) with the same applied electric field. It is found that both the poling in the PZT and copolymer improves for the case $\sigma_m = 10^{-14}$ $\Omega^{-1}m^{-1}$. The simulated behaviors for P_i and P_m with $\sigma_m = 10^{-11}\Omega^{-1}m^{-1}$ are similar to the case for $\phi = 0.1$ (i.e., PZT is nearly fully poled, whilst the copolymer is poorly polarized). The comparison between Figs. 1a and 1b then clearly reveals that the PZT inclusion is difficult to pole if the polymer in the composite is highly insulating, especially for small ϕ. Thus, experimental techniques do

exist to increase σ_m to facilitate poling [1, 6]. Also note from the figures that E_i and E_m take time to develop to a high value under an applied dc field. The poling time should therefore be sufficient to allow steady state to be reached. Our simulations show that an hour of poling time is about sufficient for both high or low σ_m samples. In addition, E_i and E_m also take time to relax back to zero under short circuit condition, hence the composite D also relaxes gradually. According to the general rule-of-thumb that the pyroelectric and piezoelectric strengths are roughly proportional to the polarization, the simulated results for D suggest the pyroelectricity and piezoelectricity may also gradually relax until $E_i = E_m = 0$.

In Fig. 2, we investigate the mechanism of poling by an ac electric field. The applied electric field is sinusoidal with 80 MV/m in magnitude and the frequency is 10 Hz. The duration of poling lasts for one and a half cycles. No matter whether $\sigma_m = 10^{-11}\Omega^{-1}\mathrm{m}^{-1}$ or $10^{-14}\Omega^{-1}\mathrm{m}^{-1}$, we find that the degree of poling in PZT is poor for both $\phi = 0.1$ [Fig. 2a] and $\phi = 0.5$ [Fig. 2b] (the simulated results for $\sigma_m = 10^{-11}\Omega^{-1}\mathrm{m}^{-1}$ and $10^{-14}\Omega^{-1}\mathrm{m}^{-1}$ overlap with each other). On the other hand, the degree of poling in the copolymer phase is better. Supposing σ_m increases

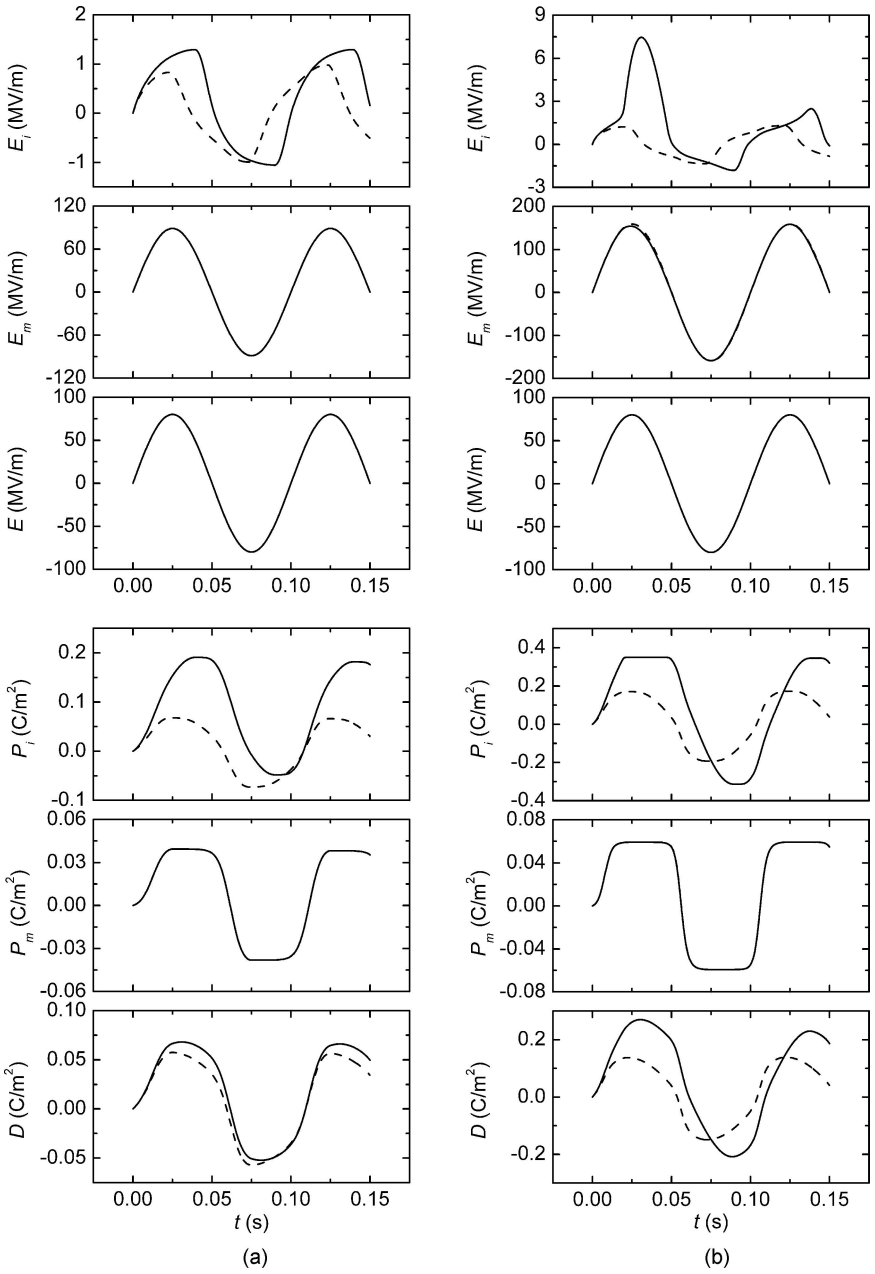

Figure 2 Simulated polarizations and electric fields of PZT/P(VDF-TrFE) composites with (a) $\phi = 0.1$, (b) $\phi = 0.5$, when the composites are polarized by an ac electric field. The dashed and solid lines denote $\sigma_m = 10^{-14}\sim10^{-11}\Omega^{-1}\mathrm{m}^{-1}$ and $\sigma_m = 2\times10^{-8}\Omega^{-1}\mathrm{m}^{-1}$ respectively.

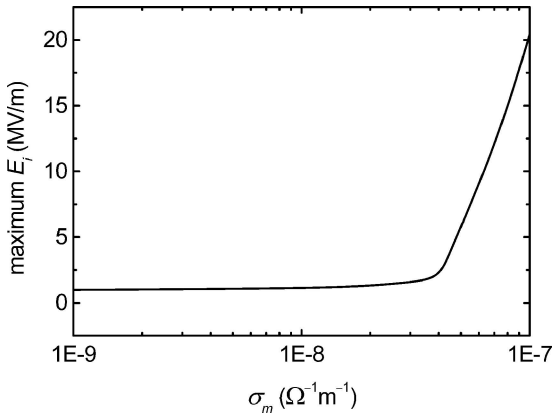

Figure 3 Variation of the maximum E_i with σ_m for a PZT/P(VDF-TrFE) composite with $\phi = 0.1$, when the composites are polarized by an ac electric field.

further to $2\times10^{-8}\Omega^{-1}\text{m}^{-1}$, the residual polarization (P_i at $t = 0.15$ s) in PZT will be high and the final P_m remains the same. Fig. 3 shows the variation of maximum E_i versus σ_m for $\phi = 0.1$, we find that there is a threshold value for σ_m which E_i is significantly increased. This confirms high σ_m facilitates poling, but such high σ_m value would not normally exist in polymeric materials at room temperature, or even at elevated temperature. It seems that ac poling is not an effective way to polarize PZT inclusions, but it has a strong effect for the polymer matrix. Also note from the figures that E_i is not zero at the end of the poling time ($t = 0.15$ s) but E_m is very close to zero, thus the relaxation in P_m after poling is expected to be not as large as in P_i.

From previous figures, we observe that dc poling is able to polarize the inclusions and matrix at different σ_m, whilst ac poling only has a strong effect in polarizing the copolymer matrix. One effective way to polarize both phases is to use a two-stage poling procedure [7, 8, 24]. Usually the sample is heated to above the Curie transition temperature of P(VDF-TrFE) and then subjected to a dc electric field for a certain duration. As the copolymer is in its paraelectric phase when the field is applied, only the ceramic phase has been polarized. This high temperature enhances σ_m and the poling in PZT is more complete [25]. After the PZT has been polarized, the composite is then cooled to below the Curie temperature of P(VDF-TrFE) and the copolymer in the composite is polarized by an ac field. This last procedure should not alter the polarization state of PZT significantly. Simulation of this poling process is shown in Figs 4 and 5.

Fig. 4 demonstrates the electric fields and polarization dynamics when both PZT and copolymer phases are polarized in the same direction. The adopted field parameters are also 60 MV/m and 80 MV/m for dc and ac poling fields. When $\sigma_m = 10^{-14}\Omega^{-1}\text{m}^{-1}$, it will not have sufficient E_i to polarize the PZT inclusion. This is similar to what we demonstrated in Fig. 1. However, we still note that the residual P_i in Fig. 1 is higher than the residual P_i (before ac poling) in Fig. 4. This suggests it is more difficult to polarize PZT inclusions in a nonferroelectric matrix. For $\sigma_m = 10^{-11}\Omega^{-1}\text{m}^{-1}$, it is shown that P_i is high after the dc poling for both $\phi = 0.1$ [Fig. 4a] and $\phi = 0.5$ [Fig. 4b]. P_m is zero because the copolymer is in the paraelectric phase. After the one and a half cycles of ac poling, the copolymer phase has been polarized to a high degree. The polarization in the PZT will be disturbed by the ac field, but its high poling degree will be restored at the end of the poling procedure. Hence, both phases are polarized to high degrees.

The above procedure may also be used to polarize the two phases in opposite directions. This has practical importance since it can reinforce piezoelectric activity and suppress pyroelectric activity to tailor for specific applications [26]. In contrast, pyroelectric activity is reinforced and piezoelectric activity is suppressed when the two phases are polarized in the same direction. Using the above two-stage poling procedure, the direction of the resulting polarization in the copolymer phase is determined by the electric field direction in the last half cycle of the ac poling field. Fig. 5 shows the simulation results for the same set of adopted σ_m and ϕ. Similar to the behavior demonstrated in Fig. 4, the degrees of poling are satisfactory for both phases for higher $\sigma_m (= 10^{-11}\Omega^{-1}\text{m}^{-1})$. One point worth noting is that, when σ_m is not sufficiently high (dashed line in Fig. 5, the residual P_i (after dc poling) could be easily switched by the ac field to the opposite direction. This may be an origin of the reduced electroactivity properties reported by Zeng *et al*. for their composite samples with oppositely poled constituents [24].

For comparison purposes, Fig. 6 shows the simulation results of composite samples subjected to a two-stage dc poling field with the two dc fields in opposite directions. It clearly shows that, for low ϕ or high ϕ and different σ_m's, the reduction of the initial polarization in the PZT phase due to the 2nd dc poling is significant and it is switched to the direction parallel to the 2nd poling field. This may be the origin of the diminished electroactivity properties reported by Ng *et al*. for their composite samples with oppositely poled constituents [17]. Indeed their composite samples with oppositely polarized phases were obtained by applying, as the final poling step, a constant poling field on the composite sample for half an hour in the reverse direction to the polarization of the pre-polarized ceramic phase, aimed at poling the copolymer phase.

Overall, the degree of poling of the constituent material depends on the poling procedure, and a higher σ_m is shown to facilitate poling. This is consistent with Sa-gong *et al*.'s conclusion [27]. A higher σ_m in composites can normally be obtained by adding conductive filler such as carbon black, or by poling at an elevated temperature. However, for a ferroelectric composite with a PTC (positive temperature coefficient of resistivity) matrix material

such as carbon black loaded polyethylene [28], a higher σ_m is achievable at a lower temperature and thus in this case the composite is more effectively poled at lower temperatures.

3.2. Effect of σ_m and measuring frequency on ε, p and d_{33} coefficients of 0-3 composites

Here, we will demonstrate that high σ_m plays a significant role in the effective ε, p and d_{33}. The adopted properties of constituents for the calculations are listed in Table II (γ in the table denotes Young's modulus). For simplicity we are only concerned about the magnitude of the pyroelectric coefficient since the matrix materials of the 0-3 composites considered below are taken as nonferroelectric. Thus although p for PZT should formally be $-330\ \mu\text{C/m}^2\text{K}$, it appears as $+330\ \mu\text{C/m}^2\text{K}$ in Table II. These adopted values are typical for a PZT/PVDF composite. Y and ν may be transformed to k and μ by using $k = Y/(3-6\ \nu)$ and $\mu = Y/(2+2\nu)$. The calculated results of ε [Equation 26], p [Equation 37] and d_{33} [Equation 68] for PZT/PVDF 0-3 composites are shown in Fig. 7. The measuring frequency for dielectric constant, pyroelectric coefficient and piezoelectric coefficient are 1 kHz, 5 mHz and 50 Hz respectively. For simplicity, only Equation 68 with μ_l is shown. In Figs 7a and c, the solid lines are based on our

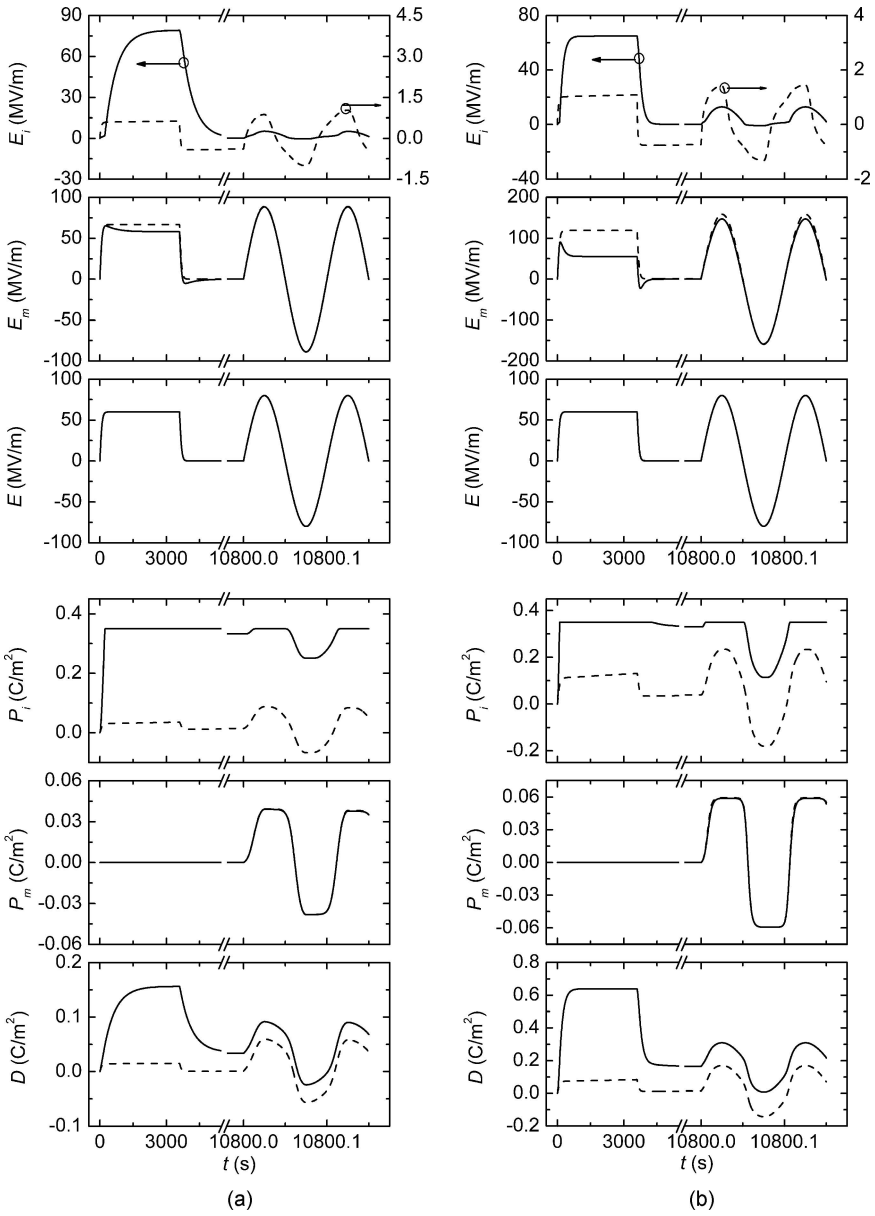

Figure 4 Simulated polarizations and electric fields of PZT/P(VDF-TrFE) composites with (a) $\phi = 0.1$, (b) $\phi = 0.5$, when the ceramic phase is first polarized by a dc electric field, then the composite is subject to an ac field to polarize the polymer phase in the same direction. The dashed and solid lines denote $\sigma_m = 10^{-14}\Omega^{-1}\text{m}^{-1}$ and $\sigma_m = 10^{-11}\Omega^{-1}\text{m}^{-1}$ respectively.

TABLE II Properties of constituents for PZT/PVDF 0-3 composites

	$\varepsilon/\varepsilon_0$	σ ($\Omega^{-1}\mathrm{m}^{-1}$)	Y (GPa)	ν	p ($\mu\mathrm{C/m^2K}$)	d_{33} (pC/N)	$-d_{31}$ (pC/N)
PZT	1200	10^{-14}	36	0.3	330	330	140
PVDF	11	varied	2.5	0.4	0	0	0

previous model [9, 11], which corresponds to $\Gamma_\varepsilon\,\varepsilon = 1$ in Equation 26 and $\Gamma_d = 1$ in Equation 68 of the present model (i.e., $\sigma_i = \sigma_m = 0$). The solid line in Fig. 7b corresponds to $\Gamma_p^{\mathrm{ac}} = 1$ in Equation 37. A typical value of conductivity for PVDF at room temperature is about 10^{-12} $\Omega^{-1}\mathrm{m}^{-1}$. The prediction based on this σ_m value overlaps with our previous model. Thus, the effect of electrical conductivity on the effective ε, p and d_{33} of conventional samples can normally be neglected at room temperature. When σ_m is increased, no notable enhancement in ε, p and d_{33} is observed until $\sigma_m = 10^{-6}$ $\Omega^{-1}\mathrm{m}^{-1}$, $\sigma_m = 10^{-11}$ $\Omega^{-1}\mathrm{m}^{-1}$ and $\sigma_m = 10^{-7}$ $\Omega^{-1}\mathrm{m}^{-1}$ respectively. More enhancement of ε, p and d_{33} is observed at higher ceramic volume fraction. Further order of magnitude increment of

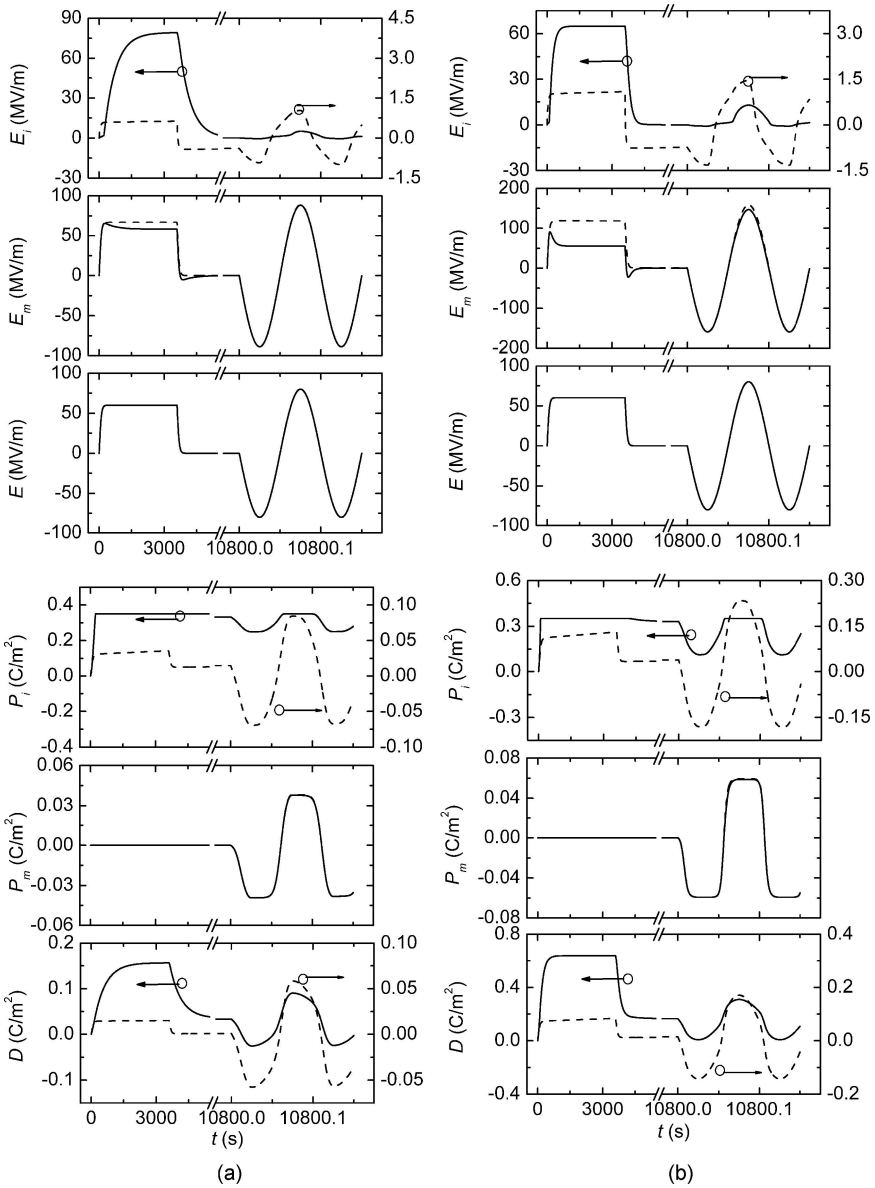

Figure 5 Simulated polarizations and electric fields of PZT/P(VDF-TrFE) composites with (a) $\phi = 0.1$, (b) $\phi = 0.5$, when the ceramic phase is first polarized by a dc electric field, then the composite is subjected to an ac field to polarize the polymer phase in an opposite direction. The dashed and solid lines denote $\sigma_m = 10^{-14}\Omega^{-1}\mathrm{m}^{-1}$ and $\sigma_m = 10^{-11}\Omega^{-1}\mathrm{m}^{-1}$ respectively.

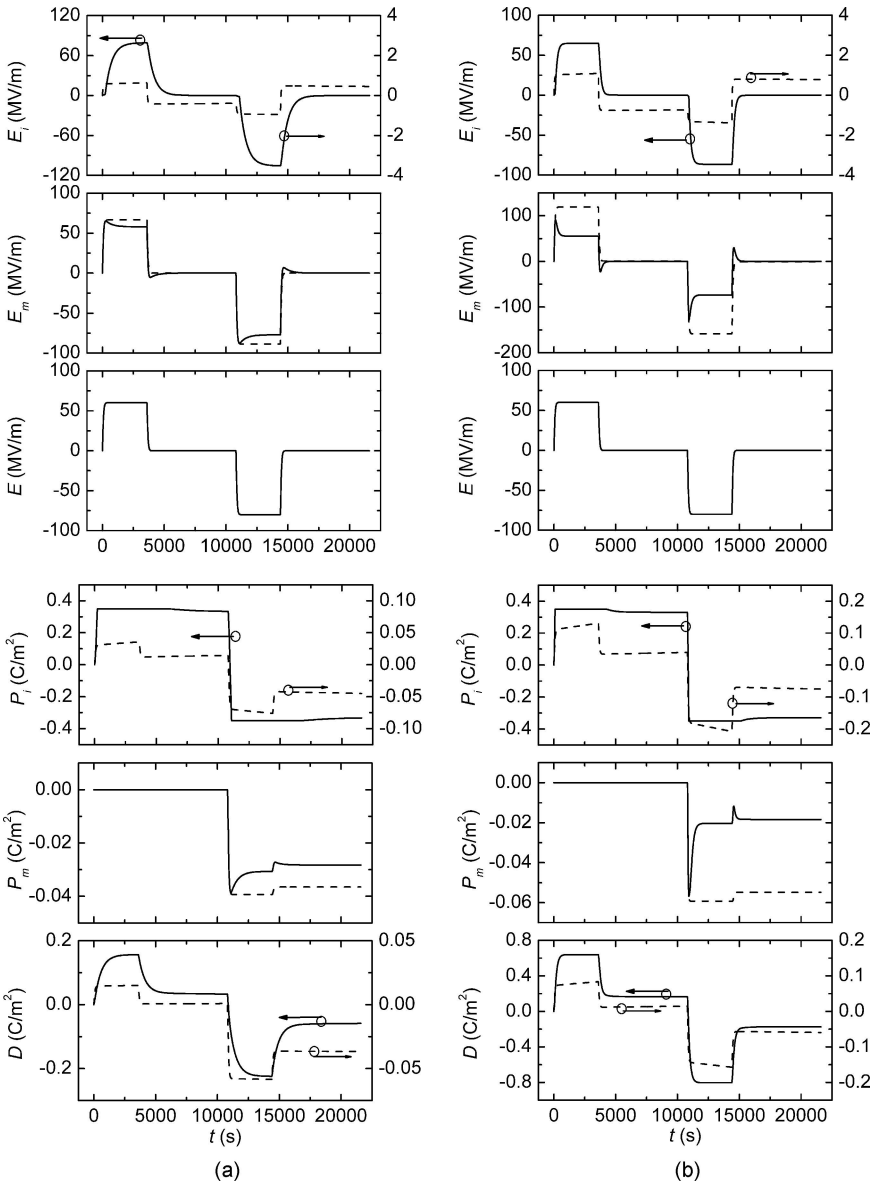

Figure 6 Simulated polarizations and electric fields of PZT/P(VDF-TrFE) composites with (a) $\phi = 0.1$, (b) $\phi = 0.5$, when the ceramic phase is first polarized by a dc electric field, then the composite is subjected to a dc field to polarize the polymer phase in an opposite direction. The dashed and solid lines denote $\sigma_m = 10^{-14}\Omega^{-1}\mathrm{m}^{-1}$ and $\sigma_m = 10^{-11}\Omega^{-1}\mathrm{m}^{-1}$ respectively.

σ_m will dramatically increase the values of ε, p and d_{33} for a given ϕ. The different σ_m values which start to "activate" the enhancement for ε, p and d_{33} are related to the different measuring frequencies. The smaller "threshold" σ_m value shown in Fig. 7b suggests electrical conductivity can affect pyroelectric measurement at lower values, whilst having least effect for permittivity measurement. This feature may be made use of in tailoring composites for higher than "normal" d_{33} constant, etc. In contrast, other approaches have been adopted in the literature to get an optimal piezoelectric response. For example, the well-known Piezo-Rubber manufactured by NTK-NGK [29–31] uses an extremely high content of PZT/$PbTiO_3$ particles (ϕ can be as large as 0.75) to obtain a resultant $d_{33} \approx 34 \sim 56$ pC/ N [32, 33], which is quite difficult to fabricate.

In Fig. 7, we demonstrate the significant effect when $\sigma_m \geq 10^{-6}\ \Omega^{-1}\mathrm{m}^{-1}$, $10^{-11}\ \Omega^{-1}\mathrm{m}^{-1}$ and $10^{-7}\ \Omega^{-1}\mathrm{m}^{-1}$ for ε, p and d_{33} respectively. It shows that all ε, p and d_{33} are very sensitive to a small change of σ_m in some region. In most of the calculations shown in Fig. 7, σ_i is taken as $10^{-14}\ \Omega^{-1}\mathrm{m}^{-1}$. In Fig. 7, the predictions for $\sigma_i = \sigma_m = 5\times10^{-6}\ \Omega^{-1}\mathrm{m}^{-1}$, $5\times10^{-11}\ \Omega^{-1}\mathrm{m}^{-1}$ and $5\times10^{-7}\ \Omega^{-1}\mathrm{m}^{-1}$ (for ε, p and d_{33} respectively) are also shown. It clearly reveals that the calculated ε, p and d_{33} values are only slightly different from the case of $\sigma_i = 10^{-14}\ \Omega^{-1}\mathrm{m}^{-1}$ with the same $\sigma_m = 5\times10^{-6}\ \Omega^{-1}\mathrm{m}^{-1}$ for ε, $5\times10^{-11}\ \Omega^{-1}\mathrm{m}^{-1}$ for p, and $5\times10^{-7}\ \Omega^{-1}\mathrm{m}^{-1}$ for d_{33}.

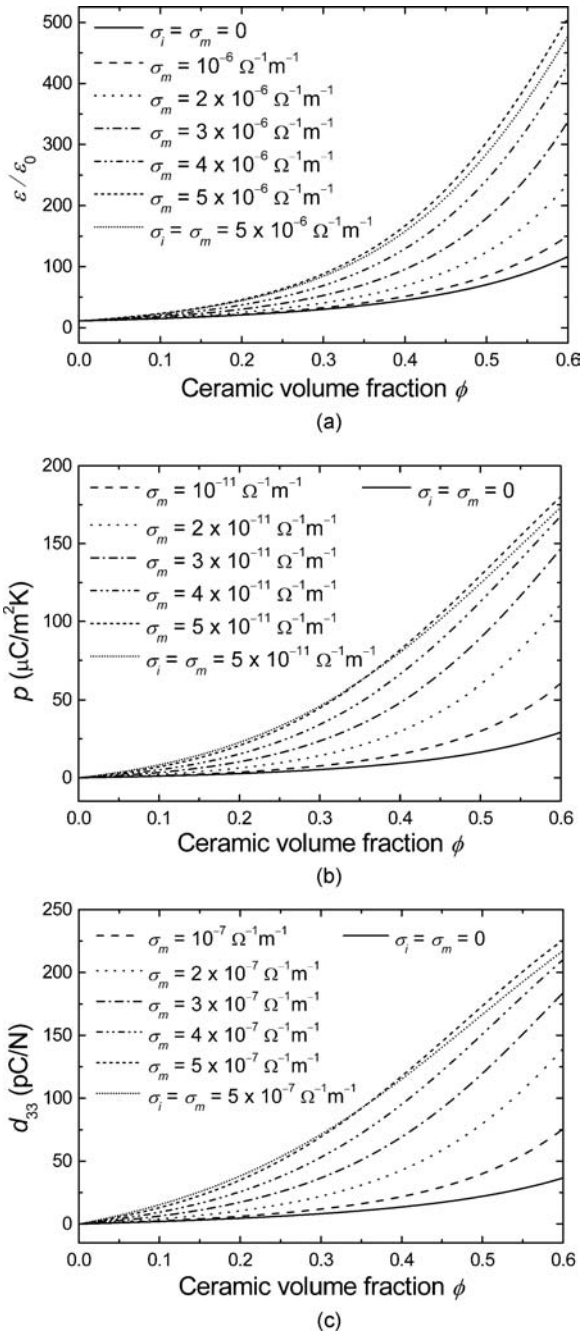

Figure 7 The variation of (a) permittivity ε [Equation 26], (b) pyroelectric coefficient [Equation 37] and (c) d_{33} constant [Equation 68] of PZT/PVDF composites with conductivity. Eqs 26, 37 and 68 with Γ's $= 1$ (solid lines) represent the constituents are perfectly insulating.

Actually, we generally find that ε, p and d_{33} are much less affected by σ_i than by σ_m.

In Equations 26, 37 and 68, τ is the governing factor which depends on the constituent permittivities, conductivities, and ϕ, rather than just σ_i or σ_m. Moreover, one can also appreciate from Equation 11 that σ_i is of lesser significance than σ_m. Fig. 8 shows the ceramic volume fraction dependence of τ with different σ_m's with $f = 50$ Hz. The figure shows that τ decreases monotonically with

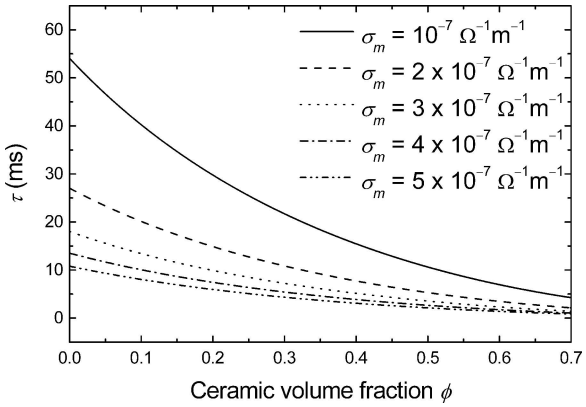

Figure 8 The variation of τ [Equation 11] of PZT/PVDF composites with conductivity in the matrix phase. The measuring frequency is 50 Hz.

ϕ for all σ_m's. Thus, ε, p and d_{33} increase with ceramic volume fraction, as noted in Fig. 7. From Fig. 8, it is found that a higher σ_m generally displaces the whole curve to lower τ values.

The effect of large σ_m essentially changes the magnitude of the induced internal electric fields as well as their phase difference with the applied electric field, modulating temperature or stress. Taking the piezoelectric measurement as an example, Fig. 9a shows a typical applied sinusoidal stress T of 50 Hz. The first three cycles of the induced electric field in the inclusion phase ($\langle E_{3i} \rangle$) are shown in Fig. 9b. Since $\langle E_3 \rangle = 0$, $\langle E_{3m} \rangle$ is out-of-phase with $\langle E_{3i} \rangle$. When $\sigma_m = 10^{-14}\ \Omega^{-1}m^{-1}$ which is typically small for conventional sample, the magnitude of $\langle E_{3i} \rangle$ is almost the same for each cycle and $\langle E_{3i} \rangle$ is out-of-phase with T. When σ_m is large, the magnitude of $\langle E_{3i} \rangle$ and its phase difference with T changes with time until steady state is reached (not shown in Fig. 9).

In Fig. 7, we have demonstrated that substantial enhancement of ε, p and d_{33} starts from $\sigma_m = 10^{-6}\ \Omega^{-1}m^{-1}$, $10^{-11}\ \Omega^{-1}m^{-1}$ and $10^{-7}\ \Omega^{-1}m^{-1}$ respectively. This enhancement continues for increasing σ_m until steady state. Fig. 10 shows the σ_m dependence in a wide range for ε, p and d_{33}. For $\sigma_m < 10^{-6}\ \Omega^{-1}m^{-1}$, ε is small and nearly independent of σ_m. Similarly for $\sigma_m < 10^{-11}\ \Omega^{-1}m^{-1}$ and $\sigma_m < 10^{-7}\ \Omega^{-1}m^{-1}$ for p and d_{33}. For σ_m between $10^{-6}\ \Omega^{-1}m^{-1}$ and $10^{-4}\ \Omega^{-1}m^{-1}$, ε significantly increases to very high values. When $\sigma_m > 10^{-4}\ \Omega^{-1}m^{-1}$, steady state is reached and no additional change in ε is observed. Since the "threshold" σ_m value for ε is very high, permittivity measurement is not expected to be significantly affected by conductivity effect for many ferroelectrics. However, conductivity effect may be notable in pyroelectricity and piezoelectricity. Fig. 10b and c demonstrate the lower "threshold" σ_m ranges (for p and d_{33}) and their limits. These apparent limits will be smaller for a lower measuring frequency.

From Equations 26, 37 and 68, the Γ's should also be sensitive to changes in the measuring frequency. Fig. 11

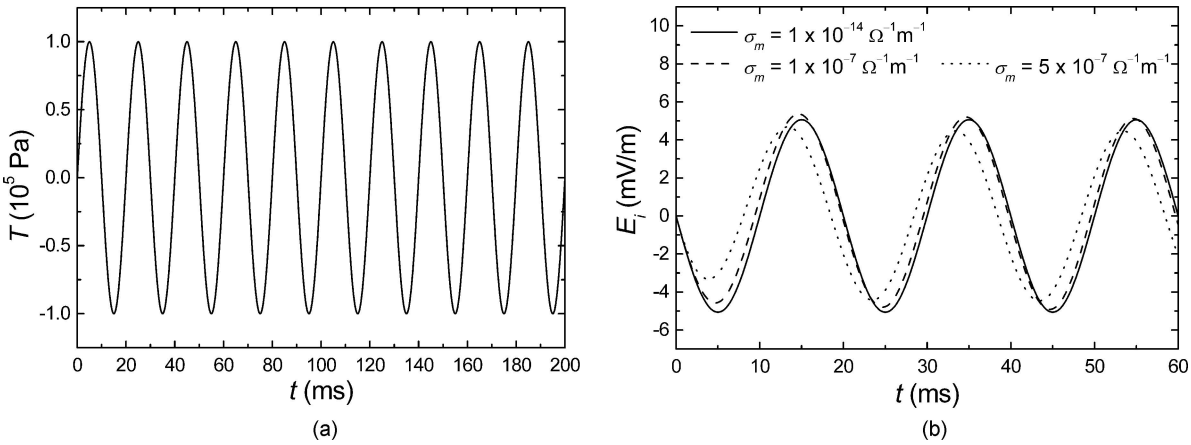

Figure 9 (a) A typical applied sinusoidal stress and (b) theoretical calculations of the induced electric field in the inclusion phase [Equation 56] for the d_{33} measurement of a PZT/PVDF composite with $\phi = 0.4$. The measuring frequency is 50 Hz.

shows the variation of ε, p and d_{33} with the measuring frequency f, assuming $\sigma_m = 5\times10^{-10}$ $\Omega^{-1}\text{m}^{-1}$ for ε, $\sigma_m = 10^{-14}$ $\Omega^{-1}\text{m}^{-1}$ for p, and $\sigma_m = 5\times10^{-10}\Omega^{-1}\text{m}^{-1}$ for d_{33}. At frequencies above 1 Hz, no notable enhancement is found for ε, and similarly for frequencies above 10 μHz and 1 Hz for p and d_{33} respectively. Further reduction in f will have an effect similar to increasing σ_m, resulting in significant enhancement of ε, p and d_{33}.

The above analyses for piezoelectricity have been confined to the d_{33} constant. Actually, the enhancement by conductivity also applies to the d_{31} [Equation 67] and d_h [Equation 69] constants. However, for the piezoelectric g_h coefficient ($\equiv d_h/\varepsilon$) which is important for hydrophone applications, piezoelectric enhancement may not be achieved by increasing σ_m, since both d_h and ε vary with σ_m and they have a common "threshold" σ_m since the "operating" frequencies are identical in this case [2]. Thus, the percentage increment of d_h must be larger than that for ε to achieve an enhanced g_h value. Summing up, with electrical conductivity considered, the new model suggested in this article yields significant effects for composite samples with high conductivity in the polymer matrix, but only minimal effects for normal composites possessing relatively low conductivity. Thus the Γ factors [Equations 26, 37 and 68] do not affect in a noticeable way the goodness of fit already obtained by many existing models [34] for ordinary composite samples. For samples possessing high σ, the effect of the Γ factors have to be included.

3.3. Comparison with experimental data for pyroelectric measurement

A previous article [6] reported that the pyroelectric coefficient of a PZT/PU 0-3 composite would be significantly increased by doping with graphite. The temperature dependence of the pyroelectric coefficient was measured for both conventional and graphite doped samples (1% by volume). The composite sample with $\phi = 0.5$ was heated at a constant rate of 1°C/min. Sakamoto *et al*. found that the pyroelectric coefficient at 303 K was 5.6 and 10.7 $\mu\text{C/m}^2$ for conventional and graphite doped samples respectively. However, the deviation of p between the two composite samples became very large at higher temperatures. Owing to the fact that the increment of p with temperature for the undoped sample is quite limited, the anomaly for the doped sample is thought to arise not solely from the increment of permittivities and pyroelectric coefficient of the constituents. The phenomenon is most likely the effect of incremental temperature on the electrical conductivity, hence the large p. Since the rate of temperature ramp is slow, the effect of conductivity of PU is thought to be significant, especially for the present situation of a graphite-doped sample.

Here we attempt to apply Equation 43 to investigate the discrepancy between the measured pyroelectric coefficients versus temperature for the foregoing PZT/PU composite system with and without graphite filler. Experimental data for pyroelectric measurement on a PZT/PU system at room temperature using the ac method can be found in ref. 19. As the dielectric and pyroelectric properties of the constituent materials provided in these articles have not been described in sufficient detail for our purposes, typical values have been adopted in our calculation, as will be explained in the next paragraph. In the present study, our theoretical calculation will only focus at the lower temperature region (303∼330 K). At the high temperature region, variations of dielectric and pyroelectric properties of the constituents will be significant and complicates the problem.

Sakamoto *et al*. have measured the permittivity of PZT at 343 K which is 1200 ε_0, but the temperature variations are not given. They have also measured the ε against temperature for PZT/PU with $\phi = 0.19$ [35]. We assume the variation of ε_i versus Θ is similar to the measurement results of PZT by Furukawa *et al*. [18]. The results of

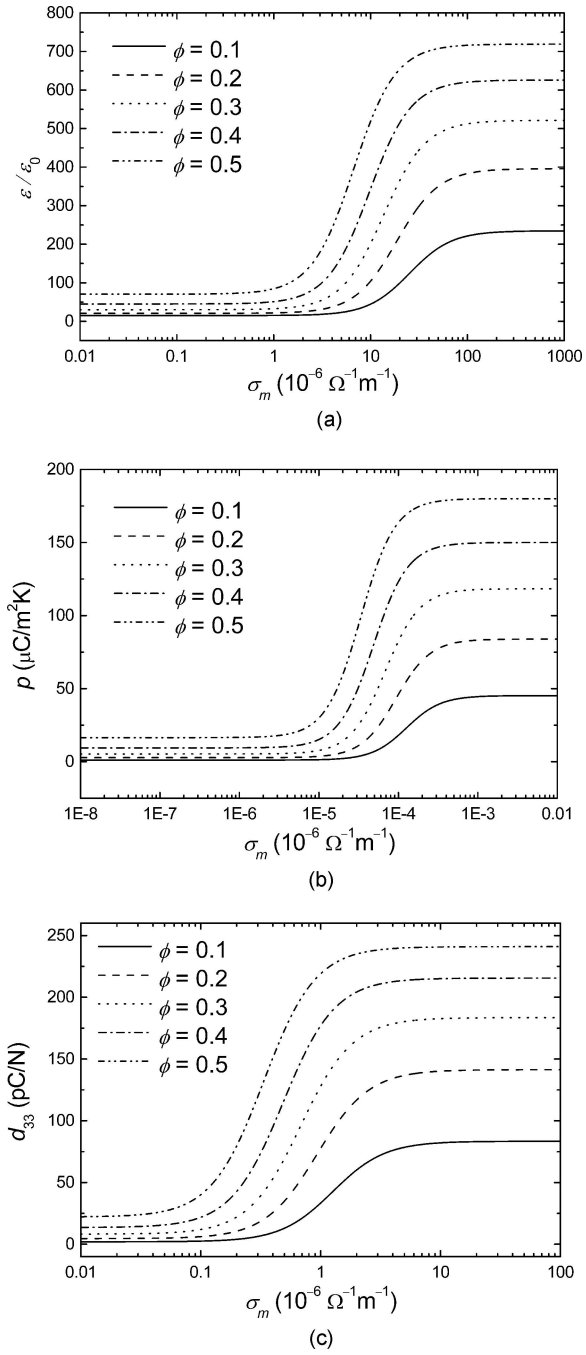

Figure 10 The variation of (a) permittivity ε [Equation 26], (b) pyroelectric coefficient [Equation 37] and (c) d_{33} constant [Equation 68] of PZT/PVDF composites with conductivity. The enhancement of ε, p and d_{33} with increasing σ_m becomes significant at 10^{-6} $\Omega^{-1}m^{-1}$, 10^{-11} $\Omega^{-1}m^{-1}$ and 10^{-7} $\Omega^{-1}m^{-1}$ respectively. They are close to maximum value for (a) $\sigma_m > 10^{-4}$ $\Omega^{-1}m^{-1}$, (b) $\sigma_m > 10^{-9}$ $\Omega^{-1}m^{-1}$ and (c) $\sigma_m > 10^{-5}$ $\Omega^{-1}m^{-1}$.

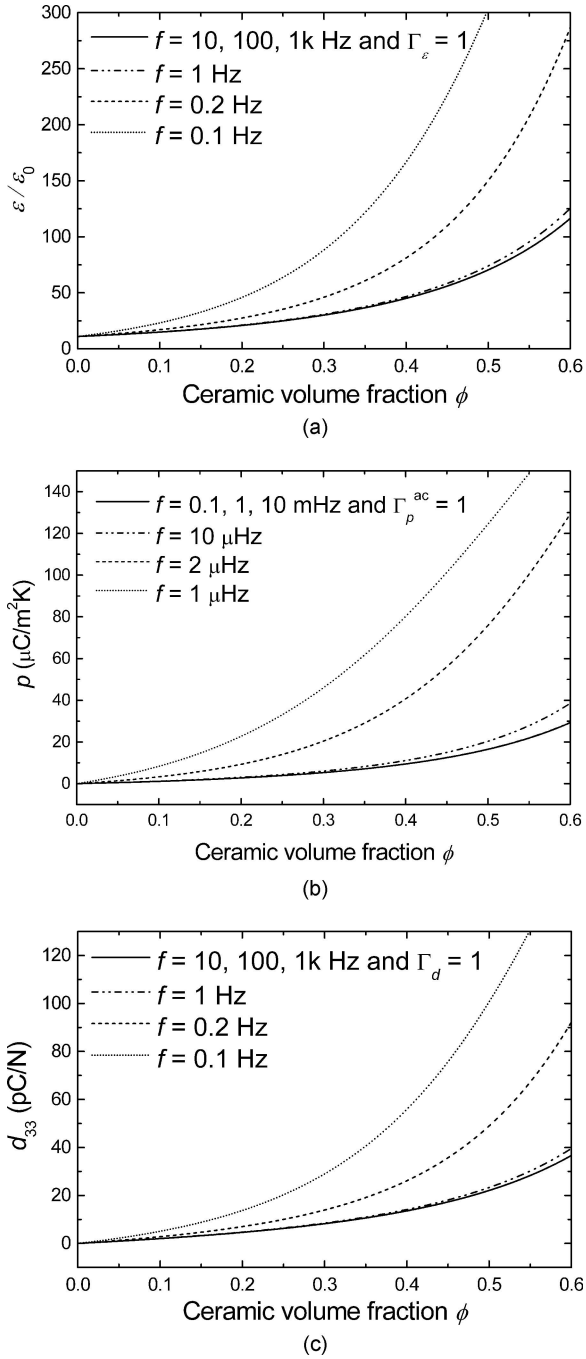

Figure 11 The variation of (a) permittivity ε [Equation 26], (b) pyroelectric coefficient [Equation 37] and (c) d_{33} constant [Equation 68] of PZT/PVDF composites with the measuring frequency. Equations 26, 37 and 68 with Γ's = 1 represent the constituents are perfectly insulating. Other lines with Γ's$\neq$1 assume the constituents possess small but finite conductivity.

permittivity against Θ by Furukawa *et al.* is then scaled in such a way that $\varepsilon_i = 1200\,\varepsilon_0$ at 343 K. For the permittivity of PU, we use Equation 27 to calculate the ε_m's from the experimental ε of PZT/PU given by Sakamoto *et al.* [35]. Fig. 12 shows our adopted temperature dependence of permittivity for the PZT and PU materials. Concerning the pyroelectric coefficients, we have $p_m = 0$ and p_i is calculated from the experimental p of undoped PZT/PU [6] with $\phi = 0.5$ [by Equation 38] and with permittivities taken from Fig. 12. In the above, we have assumed Sakamoto *et al.*'s measurement on PZT (permittivity measurement) and undoped PZT/PU (permittivity and pyroelectric measurement) is not affected by conductivity effects, so that Equations27and 38 may be employed. The temperature

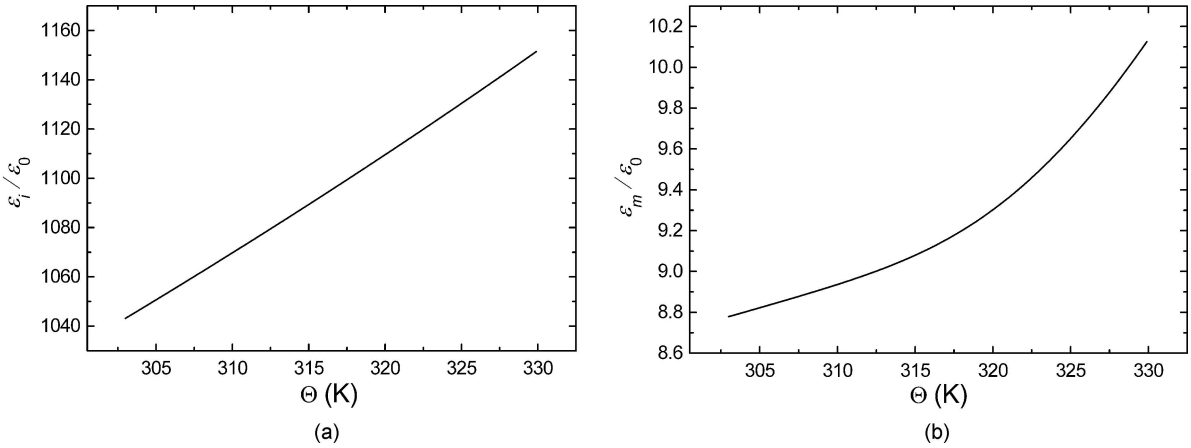

Figure 12 Temperature dependence of dielectric constant for (a) PZT ceramic, (b) PU polymer.

profile of the pyroelectric coefficient for PZT is shown in Fig. 13.

Theoretical prediction based on Equation 43 with the above constituent properties is shown in Fig. 14. When $\sigma_m = 10^{-14}\ \Omega^{-1}\mathrm{m}^{-1}$ which is small, the predicted line is very close to the experimental data for undoped PZT/PU. When σ_m is increased to $3\times10^{-13}\ \Omega^{-1}\mathrm{m}^{-1}$, we notice that, apart from the high temperatures ($\Theta > 320$ K), the general trend of p versus Θ for graphite doped PZT/PU has been reproduced by the present model incorporating conductivity. The discrepancy between the prediction and measured values may suggest the increment of σ_m with temperature should be included for higher temperature range. To investigate this, we adopt the following formula [36]

$$\sigma_m = C_1 + C_2 \exp\left(\frac{-U_{av}}{k_b\Theta}\right), \tag{86}$$

where

$$C_1 = \frac{m_b\sigma_m(\Theta_L) - m_a\sigma_m(\Theta_H)}{\sigma_m(\Theta_L) - \sigma_m(\Theta_H)}, \tag{87}$$

$$C_2 = \frac{m_b - m_a}{\sigma_m(\Theta_L) - \sigma_m(\Theta_H)}, \tag{88}$$

and $m_a = \exp(-U_{av}/k_b\Theta_L)$, $m_b = \exp(-U_{av}/k_b\Theta_H)$. U_{av} is the activation energy and k_b is the Boltzmann constant. Assume σ_m increases with temperature from 3×10^{-13} $\Omega^{-1}\mathrm{m}^{-1}$ (at $\Theta_L = 303$) to 6×10^{-13} $\Omega^{-1}\mathrm{m}^{-1}$ (at $\Theta_H = 330$) and $U_{av} = 2$ eV, the result shows excellent agreement between the prediction (solid line) and the experimental data for graphite doped PZT/PU. All in all, the consideration of electrical conductivity seems to provide a good understanding to the pyroelectric experimental results of Sakamoto *et al*.

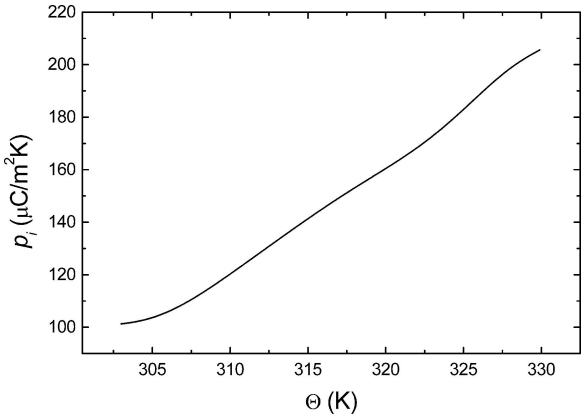

Figure 13 Temperature dependence of pyroelectric coefficient for PZT ceramic.

The present formulation neglects the loss components of the elastic and pyroelectric properties in the constituents. In the case that the loss components are also considered, all constituent parameters involved should take on complex values, and the final expressions would become much more complicated [37]. Nevertheless, an increased matrix conductivity will generally give higher, undesirable losses which need to be taken into account in considering applications. Thus, it is usually not worthwhile to make excessively conducting composites solely for rapid poling. This has been reported and discussed in the literature [27, 38]. On the other hand, manipulation of conductivity in piezoelectric and pyroelectric composites is useful for a number of devices. For instance, the damping characteristics of a mechanical composite damper can be tailored by changing the conductivity through doping the matrix [39]. For pyroelectric sensor applications, the gate voltage to the MOSFET used as a signal amplifier can be fed through the conductive composite to avoid the need for a high resistance gate resistor which is difficult and costly to realize in an integrated circuit [40]. The methodology and results of

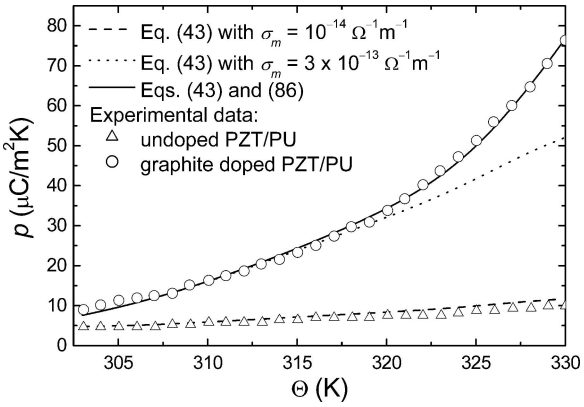

Figure 14 Theoretical prediction by Equation 43 is compared with the experimental data of Sakamoto *et al*. (see ref. 6) for the temperature dependence of p of a PZT/PU composite. The sample was heated at a constant rate of 1°C/min.

the present paper will certainly be of value for designing conducting composites for new applications.

4. Conclusions

The significance of electrical conductivities in ferroelectric 0-3 composites have been considered in this article. We have modeled the polarization behavior of ceramic/polymer 0-3 composites with different poling procedures. Our simulations suggest that higher σ_m facilitates poling. To obtain optimal poling of a ferroelectric-ferroelectric PZT/P(VDF-TrFE) composite, a two stage poling procedure with dc poling at evaluated temperature followed by an ac poling is highly advantageous. We have also calculated the effect of electrical conductivity on the dielectric, pyroelectric and piezoelectric properties. New explicit expressions have been derived for ε, p, and the d_{33}, d_{31} and d_h coefficients. A high conductivity in the matrix phase can alter the internal fields in a ferroelectric composite and allows the accumulation and dissipation of free charge at the matrix-inclusion interfaces. This can significantly enhance the permittivity, pyroelectric and piezoelectric coefficients of ferroelectric 0-3 composites. A high σ_m value may be induced by graphite doping and evaluated temperature. The permittivity ε, pyroelectric p and piezoelectric d constants will start to be noticeably enhanced when σ_m is larger than some threshold values and reach saturation beyond a certain σ_m. Comparison of our theoretical results with the experimental data of Sakamoto *et al*. show fairly good agreement, when σ_m is assumed to increase exponentially with temperature. The electrical conductivity effect is quite likely responsible for the reported anomalously high pyroelectric values in their work.

Acknowledgment

This work was partially supported by the Center for Smart Materials of The Hong Kong Polytechnic University.

References

1. X. D. CHEN, D. B. YANG, Y. D. JIANG, Z. M. WU, D. LI, F. J. GOU and J. D. YANG, *Sensor Actuat. A-Phys.* **65** (1998) 194.
2. C. K. WONG and F. G. SHIN, *J. Appl. Phys.* **97** (2005) 4111.
3. Y. T. OR, C. K. WONG, B. PLOSS and F. G. SHIN, *ibid.,* **93** (2003) 064112.
4. *Idem*., *ibid.,* **94** (2003) 3319.
5. T. FURUKAWA, *IEEE Trans. Electr. Insul*. **24** (1989) 375.
6. W. K. SAKAMOTO, P. MARIN-FRANCH and D. K. DAS-GUPTA, *Sensor Actuat. A-Phys.* **100** (2002) 165.
7. K. W. KWOK, C. K. WONG, R. ZENG and F. G. SHIN, *Appl. Phys. A: Mater. Sci. Process* **81** (2005) 217.
8. B. PLOSS, B. PLOSS, F. G. SHIN, H. L. W. CHAN and C. L. CHOY, *Appl. Phys. Lett.* **76** (2000) 2776.
9. Y. M. POON and F. G. SHIN, *J. Mater. Sci.* **39** (2004) 1277.
10. K.-H. CHEW, F. G. SHIN, B. PLOSS, H. L. W. CHAN and C. L. CHOY, *J. Appl. Phys.* **94** (2003) 1134.
11. C. K. WONG, Y. M. POON and F. G. SHIN, *ibid.,* **90** (2001) 4690.
12. C. K. WONG, Y. M. WONG and F. G. SHIN, *ibid.,* **92** (2002) 3974.
13. S. L. MILLER, R. D. NASBY, J. R. SCHWANK, M. S. RODGERS and P. V. DRESSENDORFER, *ibid.* **68** (1990) 6463.
14. S. L. MILLER, J. R. SCHWANK, R. D. NASBY and M. S. RODGERS, *ibid.* **70** (1991) 2849.
15. C. J. DIAS and D. K. DAS-GUPTA, *IEEE Trans. Dielectr. Electr. Insul.* **3** (1996) 706.
16. B. PLOSS, B. PLOSS, F. G. SHIN, H. L. W. CHAN and C. L. CHOY, *ibid.* **7** (2000) 517.
17. K. L. NG, H. L. W. CHAN and C. L. CHOY, *IEEE Trans. Ultrason. Ferroelectr. Freq. Control* **47** (2000) 1308.
18. T. FURUKAWA, K. FUJINO and E. FUKADA, *Jpn. J. Appl. Phys.* **15** (1976) 2119.
19. K. S. LAM, Y. W. WONG, L. S. TAI, Y. M. POON and F. G. SHIN, *J. Appl. Phys.* **96** (2004) 3896.
20. C. K. WONG, Y. M. POON and F. G. SHIN, *ibid.* **93** (2003) 487.
21. Z. HASHIN, *J. Appl. Mech.* **29** (1962) 143.
22. R. M. CHRISTENSEN, in "Mechanics of Composite Materials" (Wiley, New York, 1979) Chap. 4.
23. Z. HASHIN and S. SHTRIKMAN, *J. Mech. Phys. Solids* **11** (1963) 127.
24. R. ZENG, K. W. KWOK, H. L. W. CHAN and C. L. CHOY, *J. Appl. Phys.* **92** (2002) 2674.
25. H. L. W. CHAN, Y. CHEN and C. L. CHOY, *Integr. Ferroelectr.* **9** (1995) 207.
26. H. L. W. CHAN, P. K. L. NG and C. L. CHOY, *Appl. Phys. Lett.* **74** (1999) 3029.
27. G. SA-GONG, A. SAFARI, S. J. JANG and R. E. NEWNHAM, *Ferroelectrics Lett.* **5** (1986) 131.
28. B. WANG, X. YI, Y. PAN and H. SHAN, *J. Mater. Sci. Lett.* **16** (1997) 2005.
29. H. BANNO, K. OGURA, H. SOBUE and K. OHYA, *Jpn. J. Appl. Phys.* **26**(suppl. 26-1) (1987) 153.
30. H. BANNO and K. OGURA, *ibid.* **30** (1991) 2247.
31. J. F. TRESSLER, S. ALKOY, A. DOGAN and R. E. NEWNHAM, *Compos. Part A—Appl. Sci.* **30** (1999) 477.

32. R. Y. TING, *Appl. Acoust.* **41** (1994) 325.
33. R. Y. TING and F. G. GEIL, in Proc. of the 7th IEEE International Symposium on Applications of Ferroelectrics, (1991), p. 14.
34. C. J. DIAS and D. K. DAS-GUPTA, *IEEE Trans. Dielectr. Electr. Insul.* **3** (1996) 706.
35. W. K. SAKAMOTO, S. KAGESAWA, D. H. KANDA and D. K. DAS-GUPTA, *J. Mater. Sci.* **33** (1998) 3325.
36. N. BRAITHWAITE and G. WEAVER, in "Electronic Materials" (Butterworth, Boston, 1990).
37. C. K. WONG, Y. M. POON and F. G. SHIN, *J. Appl. Phys.* **92** (2002) 3287.
38. A. SAFARI, G. SA-GONG, J. GINIEWICZ and R. E. NEWNHAM, in Proceedings of the 21st University Conference on Ceramic Science, (1986) Vol. 20 p. 445.
39. Y. SUZUKI, K. UCHINO, H. GOUDA, M. SUMITA, R. E. NEWNHAM and A. R. RAMACHANDRAN, *J. Ceram. Soc. Jpn.* **99** (1991) 1096.
40. B. PLOSS, Y. W. WONG and F. G. SHIN, Ferroelectrics [to appear in a special issue of Ferroelectrics for the Fourth Asian Meeting on Ferroelectrics (AMF-4)].